Supplement of Atmos. Chem. Phys., 22, 5877–5924, 2022
https://doi.org/10.5194/acp-22-5877-2022-supplement

Atmospheric Chemistry and Physics
Open Access
EGU

Supplement of

Overview: On the transport and transformation of pollutants in the outflow of major population centres – observational data from the EMeRGe European intensive operational period in summer 2017

M. Dolores André et al.

Correspondence to: M. Dolores Andrés Hernández (lola@iup.physik.uni-bremen.de)

Supplementary Information

S1 List of institutions involved in EMeRGe

Project Partners			
Institution	**Head of Department**	**Principal Investigator**	**Link**
University of Bremen Institute of Environmental Physics: - Physics and Chemistry of the Atmosphere	Prof. Dr. John P. Burrows	Prof. Dr. John P. Burrows / Dr. Maria Dolores Andrés Hernández	www.iup.uni-bremen.de
University of Bremen LAMOS - Laboratory for Modeling and Observation of the Earth System	Prof. Dr. Mihalis Vrekoussis	Prof. Dr. Mihalis Vrekoussis / (in cooperation with Dr. Andrea Pozzer_MPI)	www.iup.uni-bremen.de/lamos
DLR - German Aerospace Center Institute of Atmospheric Physics	Prof. Dr. Markus Rapp	Dr. Hans Schlager / Dr. Helmut Ziereis / Dr. Daniel Sauer	www.dlr.de/pa
Max Planck Institute for Chemistry Particle Chemistry	Prof. Dr. Stephan Borrmann	Dr. Johannes Schneider	www.mpic.de/
Max-Planck-Institute for Chemistry Multiphase Chemistry	Prof. Dr. Ulrich Pöschl	Dr. Mira Pöhlker	www.mpic.de
Johannes Gutenberg University Mainz Institute for Atmospheric Physics: - Aerosol and Cloud Physics	Prof. Dr. Stephan Borrmann	Prof. Dr. Stephan Borrmann	www.ipa.uni-mainz.de
Heidelberg University Institute of Environmental Physics: - Tropospheric Chemistry	Prof. Dr. Ulrich Platt	Prof. Dr. Ulrich Platt / Dr. Denis Pöhler	www.iup.uni-heidelberg.de
Heidelberg University Institute of Environmental Physics: - Atmospheric Radiation and Applications	Prof. Dr. Klaus Pfeilsticker	Prof. Dr. Klaus Pfeilsticker	www.iup.uni-heidelberg.de/
University of Wuppertal Institute for Atmospheric and Environmental Research	Prof. Dr. Ralf Koppmann	Prof. Dr. Ralf Koppmann / Dr. Marc Krebsbach	www.iau.uni-wuppertal.de
Karlsruhe Institute of Technology (KIT) Institute of Meteorology and Climate Research: - Atmospheric Trace Gases and Remote Sensing	Prof. Dr. Peter Braesicke	Dr. Andreas Zahn / Dr. Harald Bönisch	www.imk-asf.kit.edu
Forschungszentrum Jülich Institute of Energy and Climate Research: Troposphere (IEK-8)	Prof. Dr. Astrid Kiendler-Scharr / Prof. Dr. Andreas Wahner	Dr. Birger Bohn	www.fz-juelich.de/iek/iek-8

S2 List of institutions involved in EMeRGe international

European Partners		
Country	**Institution**	**Link**
Belgium	**KMI** - Royal Meteorological Institute of Belgium	www.meteo.be
France	**CNRS** - French National Centre for Scientific Research	www.cnrs.fr
	University of Lille	www.univ-lille1.fr
Germany	**DWD** - German Meteorological Service	www.dwd.de
	IASS - Institute for Advanced Sustainability Studies	www.iass-potsdam.de www.uc2-program.org
	TROPOS - Leibniz Institute for Tropospheric Research	www.tropos.de
Greece	**Aristotle University of Thessaloniki**	www.auth.gr
	FORTH - Foundation for Research and Technology - Hellas	www.forth.gr
	IERSD - Institute for Environmental Research and Sustainable Development, National Observatory of Athens	www.iersd.noa.gr
	National Technical University Of Athens	www.ntua.gr
	NOA - National Observatory of Athens	www.noa.gr
	PANACEA - Panhellenic infrastructure for Atmospheric Composition and Climate Change	panacea-ri.gr
	University of Crete	www.uoc.gr
Ireland	**UCC** - University College of Cork	www.ucc.ie
Italy	**CNR-ISAC** - National Research Council of Italy, Institute of Atmospheric Sciences and Climate	www.isac.cnr.it
	CNR-IMAA - National Research Council of Italy **I**stituto di Metodologie per l'Analisi Ambientale	www.imaa.cnr.it
	University of L'Aquila	www.univaq.it
	University of Naples Federico II	www.unina.it
	University of Rome La Sapienza	www.phys.uniroma1.it
	University of Salento, Mathematics and Physics Department	www.unisalento.it
Netherlands	**KNMI** - Royal Netherlands Meteorological Institute	www.knmi.nl
Spain	**CEAM** – Mediterranean Center for Environmental Studies	www.ceam.es
	CIEMAT- Centro de Investigaciones Energéticas, Medioambientales y Tecnológicas	www.ciemat.es
	IDAEA-CSIC – Spanish National Research Council, Institute of Environmental Assessment and Water Research	www.idaea.csic.es

	University of Granada	www.ugr.es
	University of Valencia	www.uv.es
	UPC - Universitat Politècnica de Catalunya	www.upc.edu
United Kingdom	**NCAS** - National Center for Atmospheric Science	www.ncas.ac.uk
	University of Hertfordshire	www.herts.ac.uk
	University of Manchester	www.manchester.ac.uk
	University of York	www.york.ac.uk
	FAAM - Facility for Airborne Atmospheric Measurements	www.faam.ac.uk
Asian Partners		
Country	**Institution**	**Link**
Japan	**Chubu University**	www.chubu.ac.jp
	Chiba University	www.chiba-u.jp
	CRIEPI - Central Research Institute of Electric Power Industry	criepi.denken.or.jp
	Fukuoka University	www.fukuoka-u.ac.jp
	JAMSTEC - Japan Agency for Marine-Earth Science and Technology,- Research Institute for Global Change (RIGC)	www.jamstec.go.jp
	JAXA - Japan Aerospace Exploration Agency	www.jaxa.jp
	JMA - Japan Meteorological Agency	www.jma.go.jp
	Kanazawa University	www.kanazawa-u.ac.jp
	Kobe University	www.kobe-u.ac.jp
	Kyushu University	www.kyushu-u.ac.jp
	MRI - Meteorology Research Institute	www.mri-jma.go.jp
	Nagoya University	www.nagoya-u.ac.jp
	Nara Womens's University, - Department of Chemistry, Biology and Environmental Science	www.nara-wu.ac.jp
	NICT - National Institute of Information and Communications Technology	www.nict.go.jp
	NIES - National Institute for Environmental Studies	www.nies.go.jp
	NIPR - National Institute of Polar Research	www.nipr.ac.jp
	Osaka Prefecture University, - Department of Applied Chemistry	www.osakafu-u.ac.jp
	Tokyo Metropolitan University	www.tmu.ac.jp
	University of Tokyo	www.u-tokyo.ac.jp
	University of Toyama	www.u-toyama.ac.jp
Peoples's Republic of China	**Peking University,** College of Environmental Sciences and Engineering	www.pku.edu.cn
	Nanjing University, School of Atmospheric Science	www.nju.edu.cn

	Jinan University, Guangzhou	www.jnu.edu.cn
Philippines	**Oscar M. Lopez Center** for Climate Change and Disaster Management Foundation	www.omlopezcenter.org
	University of the Philippines Diliman, - IESM - Institute of Environmental Science and Meteorology	upd.edu.ph
	HUFS - Hankuk University of Foreign Studies, - Department of Environmental Science	www.hufs.ac.kr
Republic of Korea	**Seoul National University** - School of Earth and Environmental Sciences), - Atmospheric & Climate Environment Laboratory	www.snu.ac.kr
	Yonsei University Atmospheric Radiation Laboratory	www.yonsei.ac.kr
	Academia Sinica **- RCEC** - Reseach Center for Environmental Changes	www.sinica.edu.tw
Taiwan (Republic of China)	**NTU** - National Taiwan University	www.ntu.edu.tw
	NCKU – National Cheng Kung University, Tainan	www.iaa.ncku.edu.tw
	AIT - Asian Institute of Technology, - SERD - School of Environment, Resources and Development	www.ait.ac.th
Thailand	**LPRU** - Lampang Rajabhat University, - Faculty of Science, Atmospheric Science and Astronomy Research Unit	www.lpru.ac.th
	NARIT - National Astronomical Research Institute of Thailand, - Near-Earth Objects, Space Weather and Earth's Climate	www.narit.or.th
	NARIT - National Astronomical Research Institute of Thailand, - Near-Earth Objects, Space Weather and Earth's Climate	www.narit.or.th
Other Partners		
Country	**Institution**	**Link**
European Union	**JRC** - EU Science Hub - Joint Research Centre, Ispra	ec.europa.eu/jrc/en/about/ jrc-site/ispra
Australia	**UOW** - University of Wollongong, - Centre for Atmospheric Chemistry	www.uow.edu.au
United States of America	**Georgia Institute of Technology,** - Earth and Atmospheric Sciences	www.gatech.edu

S3 Model simulations used for flight planning

S3.1 CAMS

CAMS (Copernicus Atmosphere Monitoring Service, http://atmosphere.copernicus.eu) is the successor of the former GEMS (Global and regional Earth-system Monitoring using Satellite and in-situ data; Hollingsworth et al., 2008) and three succeeding MACC (Monitoring Atmospheric Composition and Climate, http://www.gmes-atmosphere.eu/) projects. It extends weather services of the ECMWF (European Centre for Medium-Range Weather Forecasts) with simulations of atmospheric trace gases and aerosols as part of its global component. Operational air quality forecasts and analyses for Europe are provided at much finer resolution through the regional component.

CAMS-global simulations of atmospheric composition are based on the C-IFS (Composition - Integrated Forecasting System; Flemming et al., 2015) of the ECMWF. C-IFS is a version of the CB05 (Carbon Bond 2005 chemistry scheme; Huijnen et al., 2010) derived from the CTM Transport Model 5 (TM5). Within C-IFS, modules of atmospheric chemistry and physical processes are integrated on-line and several ground-based and satellite data are assimilated (see Inness et al., 2015). For EMeRGe in Europe, CO passive tracer (i.e., no chemical loss or production) forecasts for the MPCs of London, the Ruhr area, Amsterdam/Rotterdam, Berlin, Po Valley, Madrid, Paris, Rome and of biomass burning from Europe, North America and Siberia were provided through the CAMS field campaign support service (https://atmosphere.copernicus.eu/scientific-field-campaign-support, see Flemming et al., 2019). In these runs either emissions from EMeRGe target cities (CO city tracer), or only BB emissions were switched on in the simulations. A stratospheric ozone tracer subject to loss in the troposphere from the CAMS operational model system was used as indicator of stratospheric versus tropospheric air masses. For flight planning and analysis of conditions for EMeRGe in Europe, the CAMS tracer output is used in addition to full atmospheric chemistry forecasts of the operational suite. The CAMS-global simulations were performed with T511L60 model resolution. The MACCity (Granier et al., 2011) emission inventory is used for anthropogenic emissions, GFASv1.2 (Kaiser et al., 2012) for near-real-time fire emissions and a climatology of MEGAN-MACC (Sindelarova et al., 2014) for biogenic emissions. Stratospheric chemistry is not implemented in C-IFS, stratospheric ozone is derived from the Cariolle scheme (Cariolle and Teyssèdre, 2007), stratospheric NO_x is implicitly constrained by fixing the HNO_3/O_3 ratio at the 10 hPa level.

S3.2 HYSPLIT

The Lagrangian Particle Dispersion Model HYSPLIT (https://www.arl.noaa. gov/hysplit/) was used to calculate the transport and dispersion of local CO emissions, accumulated over 6 days. The simulated CO concentrations do not include accumulated "background" values due to the much longer lifetime of CO and are thus not to be compared with absolute concentrations but rather with "enhancements" inside of local plumes. HYSPLIT was driven by meteorology data from operational ECMWF forecast (0-11 hours forecast, 12-hourly update, interpolated at 0.1 deg horizontally, pressure levels, 1-hourly output). CO emission rates were taken from the EDGAR HTAP V2 emission inventory, http://edgar.jrc.ec.europa.eu/htap_v2/). Dry and wet deposition can be modelled, but no chemical reactions. No convection, only large-scale vertical movements as provided by the meteorological data set used as input. The computation (core-model) and the visualisation (post-processing) are controlled by a specific client-server infrastructure developed at DLR-IPA for campaign-support as well as post-campaign analysis.

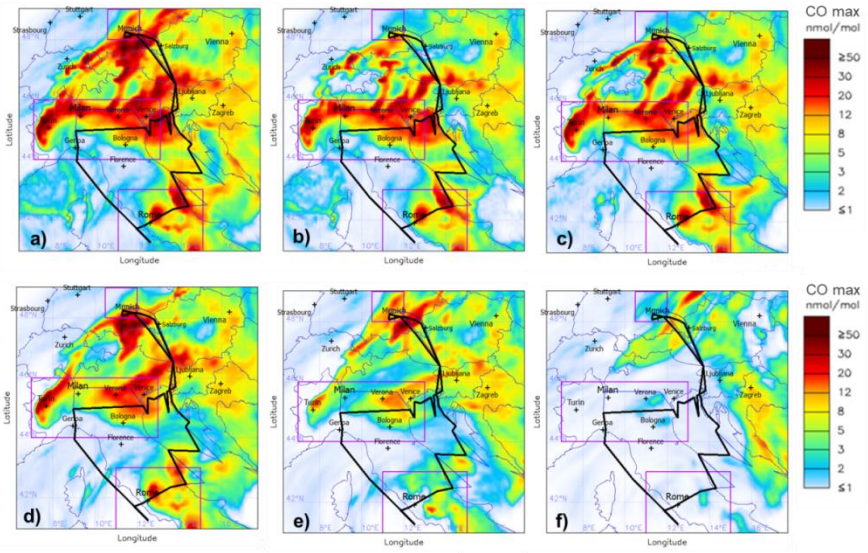

Figure S3.2.1: Example of HYSPLIT forecast for the flight planning on 20 July 2017 resulting from a 6 days accumulation of CO from selected EU metropolitan areas, as indicated by the squares (in purple). In this example the ECWMF forecast is initialised on 19 July 2017 at 12 UTC for a) total maximum volume mixing ratio (VMR) between ground level and 3200m, b) mean VMR between 300-700m above ground level (agl), c) mean VMR between 700-1200m agl d) mean VMR between 1200-1800m agl, e) mean VMR between 1800-2500m agl, and f) mean VMR between 2500-3200m agl; all averaged from 12 to 15 UTC. The flight track is superimposed in black.

S4 Perfluorocarbon tracer experiments

Tracer experiments were performed during EMeRGe using perfluorocarbon compounds (PFC). PFCs are suitable tracers as they are chemically inert, do not interact with aerosol and clouds, have a very low background in the atmosphere (~10 ppqv), and can be detected at mixing ratios as low as 1 ppqv. The tracer experiments involved the release of a mixture of PFCs at a site close to the centre of a MPC. These experiments establish Lagrangian connections between MPC centres and HALO measurements downwind. They supported studies on the formation of secondary gases and aerosol particles from the primary emissions in the pollution plumes. In addition, tracer experiments were used to test the dispersion parametrisations in transport models.

During the EMeRGe IOP in Europe, PMCH (C_7F_{14}, 350 amu) was the PFC used to tag polluted air masses at the release sites. The tracer was sampled on sorption tubes on-board and subsequently analysed in the laboratory, as described in Ren et al., (2013, 2015). The limit of detection (LOD) and limit of quantification (LOQ) of the PFC analysis system for sorption tube samples loaded for 3 min are 0.7 ppqv and 2 ppqv, respectively. The precision and accuracy are 6% and 11%, respectively. Three tracer releases were performed: two in the city centre of London at the Imperial College on 17 and 26 July 2017 and one in the industrial Ruhr region, at the University of Wuppertal on 26 July 2017 in Germany. The HALO flights and pattern for the tracer sampling in the plumes downstream were optimised with respect to the time of the tracer releases by using HYSPLIT tracer dispersion forecasts. Post-campaign comparisons of the tracer measurements were performed with HYSPLIT and FLEXPART.

S5 BAHAMAS

Basic meteorological and aircraft data were provided from DLR-FX developed BAHAMAS (BAsic HALO Measurement And Sensor System) instrument at 1 s and 0.1 s time resolution in NASA Ames and NetCDF (Network Common Data Form) format. In the standard configuration BAHAMAS acquires data from airflow and thermodynamic sensors as well as from the aircraft avionics and a high-precision GNSS/IMU (Global Navigation Satellite System / Inertial Measurement Unit) system to derive basic meteorological parameters like pressure, temperature, humidity and the 3-D wind vector as well as aircraft position and altitude.

High accuracy water vapour concentration and further derived humidity parameters are measured by the SHARC (Sophisticated Hygrometer for Atmospheric ResearCh) instrument, installed inside of BAHAMAS, based on direct absorption measurement by a tunable diode laser (TDL) system.

Typical absolute accuracy of the basic meteorological data is 0.3hPa for static pressure, 0.5 K for temperature, 0.5 m s^{-1} for east and north and 0.3 m s^{-1} for vertical wind component, 10 m for pressure altitude, 4.2 m for altitude above mean sea level (see Schumann, 2020) and 5 % ± 1 ppmv for water vapour volume mixing ratio from SHARC (see Schulz et al., 2018).

Table S5.1: BAHAMAS 1Hz and 10Hz standard output data.

Data	**Parameter [unit]**	**Data**	**Parameter [unit]**
Time	Seconds after midnight (UTC)	Meteorological	Pressure altitude [m]
Aircraft position and attitude	WGS84 altitude [m]		Calculated altitude above sea level from meteorological data [m]
	WGS84 latitude and longitude [°]		Static pressure [hPa]
	root mean square value for x-, y- and z-position [m]		Dynamic pressure [hPa]
	Ground speed [m s^{-1}]		Static air temperature [K]
	Calculated true air speed [m s^{-1}]		Total air temperature [K]
	Mach number [Ma]		Potential temperature [K]
	North-, East-, up-velocity [m s^{-1}]		Virtual temperature [K]
	x-, y- and z-axis acceleration [m s^{-2}]		Virtual potential temperature [K]
	Vertical acceleration [m s^{-2}]		Dewpoint temperature [K]
	Angle of attack [°]		Absolute humidity [g m^{-3}]
	Angle of sideslip [°]		Relative humidity respect to water [%]
	Actual track angle [°]		H_2O volume mixing ratio [µmol mol^{-1}]
	True heading [°]		H_2O mass mixing ratio [g kg^{-1}]
	Pitch angle [°]		Horizontal wind direction [°]
	Roll angle [°]		Horizontal windspeed [m s^{-1}]
	Yaw rate [° s^{-1}]		Wind vector North component [m s^{-1}]
	Pitch rate [° s^{-1}]		Wind vector East component [m s^{-1}]
	Roll rate [° s^{-1}]		Wind vector vertical component [m s^{-1}]

S6 Complementary observations within EMeRGe international

S6.1 Airborne observations

The Facility for Airborne Atmospheric Measurements (FAAM, see www.faam.ac.uk) from the UK Natural Environment Research Council (NERC) joined the EMeRGe IOP in Europe. It made a set of flights around London in the Southeast of England in the UK.

The research flight on 13 July 2017 was dedicated to common and simultaneous measurements of HALO and FAAM in a so-called blind intercomparison exercise. In total, 24 instruments were operated on the two aircraft and provided data for the comparison. The data obtained were uploaded under blind conditions and evaluated by an external referee (see S7).

The Italian Sky Arrow Environmental Research Aircraft (see Gioli et al., 2006) from the National Research Council of Italy (CNR) undertook additionally two research flights up to 2000 m over the city of Rome (Italy) concurrently with the HALO overpass flight on 11 July 2017. The aircraft was equipped with instrumentation targeting some aerosol parameters (total number and size distribution), gas concentrations (CO_2, O_3, H_2O) and key meteorological data (temperature, pressure and wind).

S6.2 Collocated ground-based observations

EMeRGe was supported by measurements from a variety of ground-based stations which complemented the HALO observations. These measurements were also used for the planning of subsequent HALO flights and occasionally for in-flight manoeuvres. For example, the European Aerosol Research Lidar Network, EARLINET (Pappalardo et al., 2014), a key component of the Aerosols, Clouds and Trace gases Research Infrastructure ACTRIS, joined as an EMeRGe international partner and provided coordinated, ground-based lidar measurements. Additional support was provided from other non-EARLINET lidar stations. Altogether, 19 stations supported the EMeRGe IOP in Europe. The specifications and location of the operated lidars as well as the coordinated measurements for each HALO flight are shown in Figure S6.2.1.

In addition, measurements from several ceilometer networks contributed to EMeRGe, in particular the German Ceilonet of DWD (Deutscher Wetterdienst), the Italian ALICEnet (Automated Lidar-Ceilometer network, https://www.alice-net.eu/) and the ceilometers of the Belgian RMI (Royal Meteorological Institute of Belgium). The RMI also provided ozone soundings from Uccle three times per week. Additional ground-based and in-situ measurements were provided from ACTRIS stations, and sun-photometer measurements from AERONET (Aerosol Robotic Network, Holben et al., 1998)

Two ground-based field campaigns deploying both remote sensing and in-situ measurements concurred with the EMeRGe IOP: ACTRIS-2 in the Po Valley, Italy (see http://actris-cimone.isac.cnr.it/), and HOUSE (High Ozone, Ultrafine particles and Secondary aerosol Episodes in urban and regional backgrounds) in Northeast Spain (see https://www.idaea.csic.es/egar/portfolio-items/house/). These data were made accessible for the analysis in the framework of EMeRGe international.

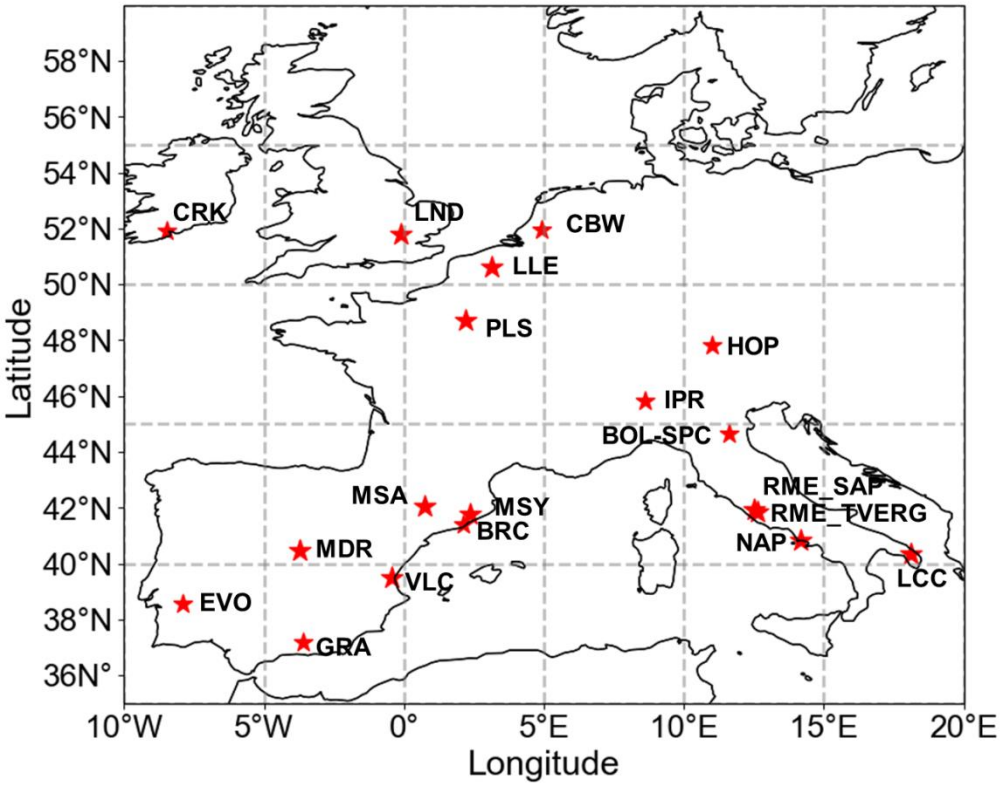

Figure S6.2.1: Coordinated lidar and ceilometer measurements during the EMeRGe campaign in Europe. Names corresponding to the abbreviations are listed in Table S6.2.1.

131 **Table S6.2.1:** Coordinated lidar and ceilometer measurements provided from EARLINET ground based stations during the
132 EMeRGe IOP in Europe, Coordinates, abbreviations and principal investigators are additionally specified Multiwavelength-
133 Polarization; MR: Multiwavelength-Raman; MPR: Multiwavelength-Polarization-Raman; PR: Polarization-Raman.

Station	Coordinates	Instrument	Principal Investigator
Barcelona (BRC)	41.386 N 2.117 E	Polarization-Lidar	J. M. Baldasano, M. Sicard
Bologna (BOL-SPC)	44.652 N 11.624 E	Polarization-Lidar	A. Boselli
Cabauw (CBW)	51.970 N 4.930 E	MPR Lidar	A. Apituley
Cork (CRK)	51.893 N -8.494 E	PR Lidar	A. Ruth
Evora (EVO)	38.568 N -7.912 E	MPR Lidar	D. Bortoli
Granada (GRA)	37.1640 N -3.605 E	MPR Lidar	L. A. Arboledas
Hohenpeissenberg (HOP)	47.802 N 11.012 E	MPR Lidar	I. Mattis
Ispra (IPR)	45.817 N 8.617 E	MPR Lidar	J.-P. Putaud
Lecce (LCC)	40.333 N 18.100 E	Multiwavelength-Lidar	M. R. Perrone
Lille (LLE)	50.612 N 3.142E	MP Lidar	P. Goloub
London (LND)	51.775 N -0.095 E	Lidar	D. Müller
Madrid (MDR)	40.456 N -3.726 E	MR Lidar	M. Pujadas
Montsec (MSA)	42.050 N 0.733 E	Ceilometer	A. Alastuey
Montseny (MSY)	41.767 N 2.350 E	Ceilometer	A. Alastuey
Naples (NAP)	40.838 N 14.183 E	MPR Lidar	N. Spinelli
Palaiseau (PLS)	48.713 N 2.208 E	MP Lidar	M. Haeffelin
Rome I (RME_SAP)	41.920 N 12.520 E	MPR Lidar	M. Cacciani
Rome II (RME_TVERG)	41.833 N 12.650 E	MR Ceilometer	D.Dionisi F. Barnaba
Valencia (VLC)	39.500 N -0.420 E	Multiwavelength-Lidar	J. L. Gómez-Amo

134

135

136

Table S6.2.2: Ground-based stations with estimated horizontal distance from HALO during the flights carried out during EMeRGe in Europe. For flight details see Sect. 3.6.

Flight number	Flight date	Ground-based station	Distance (km)
E-EU-03	11.07	Bologna (BOL)	70
		Hohenpeissenberg (HOP)	20
		Ispra (IPR)	35
		Lecce (LCC)	350
		Naples (NAP)	170
		Rome (RME)	0
E-EU-04	13.07	Hohenpeissenberg (HOP)	135
E-EU-05	17.07	Cabauw (CBW)	185
		Cork (CRK)	390
		Lille (LLE)	40
		London (LND)	160
		Palaiseau (PLS)	115
E-EU-06	20.07	Bologna (BOL)	45
		Ispra (IPR)	100
		Lecce (LCC)	395
		Naples (NAP)	170
		Rome (RME)	0
E-EU-07	24.07	Barcelona (BRC)	55
		Hohenpeissenberg (HOP)	25
		Ispra (IPR)	155
		Madrid (MDR)	530
		Montsec (MSA)	185
		Montseny (MSY)	50
E-EU-08	26.07	Cabauw (CBW)	90
		Hohenpeissenberg (HOP)	130
		Lille (LLE)	85
		London (LND)	80
		Palaiseau (PLS)	106
E-EU-09	28.07	Barcelona (BRC)	50
		Granada (GRA)	435
		Hohenpeissenberg (HOP)	85
		Montsec (MSA)	50
		Montseny (MSY)	10
		Valencia (VLC)	60

137

138

S6.3 Satellite observations

Near real-time tropospheric NO_2 columns from the GOME-2 instruments on MetOp-A (GOME2-A; 40 km x 40 km resolution) and MetOp-B (GOME2-B; 80 km x 40 km resolution) as well as OMI (13 km x 24 km resolution at nadir) on NASA Aura were provided in July and August 2017 to support flight planning and quick-look interpretation of the EMeRGe IOP observations. NO_2 columns are calculated using the method described in Richter et al., (2005, 2011), and Hilboll et al., (2014). The retrievals use GOME-2 lv1 data provided by EUMETSAT and OMI lv1 data provided by NASA. They are not official GOME-2 / OMI data products. The plots were usually available 6 hours after the measurement (https://www.iup.uni-bremen.de/doas/emerge.htm).
In addition, daily values of the aerosol optical thickness (AOT) at 0.55 μm were retrieved from the Spinning Enhanced Visible and Infrared Imager (SEVIRI) on-board the Meteosat Second Generation (MSG) satellite. The spatial and temporal resolutions for the SEVIRI AOT product are 3 km at nadir and 15 minutes, respectively. The SEVIRI AOT product over land (SMAOL_AOT.v1.3.6) and ocean (SEV_AER-OC-L2.v1.04) (see Thieuleux et al., 2005; Bréon et al., 2011) are merged and post-processed by using the eXtensible Bremen Aerosol/cloud and surfacE parameters Retrieval (XBAER) algorithm to minimise potential cloud contamination (Mei et al., 2017a, 2017b).

S7 HALO-FAAM intercomparison exercise

HALO and FAAM research aircrafts flew in close formation for 1.6 hours around noon in the northern part of a restricted airspace, “TRA Allgaeu”, between Augsburg and Ulm, in Southern Germany. HALO and FAAM flew closely together in a racetrack pattern on three flight levels. The formation flight started at FL150 (4572 m) in a rather dry and clean troposphere and ended at FL 40 (1219 m) in a more polluted convective boundary layer. Table S7.1 summarises the instrumentation on-board FAAM available for comparison. In total, 24 instruments were operated on the two aircraft and provided data for the comparison.
The uploaded data were evaluated by an external referee (see Schumann, 2020), accessible via https://zenodo.org/record/4427965). The data collection identified 28 parameters sampled on both aircrafts and further 13 pairs of data from sampling on either HALO or FAAM. In addition, observational data were collected from the German Weather Service at the observatory Hohenpeissenberg (47°48’N, 11°01’E), located about 1000 m above sea level and 40 to 100 km downstream of the aircraft track in the TRA Allgaeu, and model results were generated from 6 models and interpolated along the common flight path. Together, the combined data set includes 221 parameters allowing for comparisons between 277 pairs of data. An overview of the measured and modelled data available for direct comparisons is provided in the following tables.

Table S7.1: FAAM instrumentation for the intercomparison exercise on 13 July 2017. NS: navigation system; SDPS: Static and dynamic pressure sensor; PtRT: platinum resistance thermometers; RH: relative humidity; C-ToF-AMS: Compact time-of-flight aerosol mass spectrometer; CPC: Condensation Particle Counter; FGGA: Fast greenhouse gas analyser; TILDAS: Tunable IR laser direct absorption spectrometer; WAS-GC-FID: Whole air canister sample - Gas chromatography - Flame-ionization detection; OA.-COS: Off axis-integrated cavity output spectroscopy, AC: Academic institution

FAAM measurements			
Species/parameters	**Acronym**	**Institution**	**Technique/Instrument**
Org, NO_3, SO_4, NH_4, Chl, Org44	AMS	Manchester AC	C-ToF-AMS
NO, NO_2	AQD	York AC	Chemiluminescence
Lon, Lat, altitude , T, U, V, W, T_DI, CO, (O_3), H_2O, P, CPC, RH	CORE	FAAM	Satellite/inertial NS, SDPS, PtRT, VUV fluorometry (CO), UV photometry (O_3), CPC
CH_4, CO_2	FGGA	NERC AC	OA-COS
Np, Dp	SMPS	Manchester AC	Scanning mobility particle sizer
rBCm, rBCn, SCn, MMD, CTTR	SP2	Manchester AC	Single particle soot photometry
C_2H_6	TILDAS	Manchester AC/York AC	Laser absorption spectrometry
C_2H_6, C_2H_4, C_3H_8, C_3H_6, C_4H_{10},C_2H_2, C_5H_{10}, C_5H_{12}, C_4H_6, C_6H_{14}, C_7H_{16}, C_6H_6, C_8H_{18}, C_8H_{18},C_7H_8	WAS-GC-FID	York AC	Off line GC-FID

Table S7.2: Overview of measured and model data available for the intercomparison exercise on 13 July 2017. x, xx, xxx denotes data from 1, 2 or 3 instruments on one aircraft, and (x): outside comparison period. Columns: HALO and FAAM: aircraft instruments; HOP: measurements at Germany Weather Service (Deutscher Wetterdienst, DWD) Hohenpeissenberg; Models: CAMS: Copernicus Atmosphere Monitoring Service model, EMAC: Global ECHAM/MESSy atmospheric climate/chemistry model, MECO: Regional air chemistry/climate model based on ECHAM/COSMO, CESM2: air chemistry version of the CAM6 model, Photo: a photochemistry equilibrium model, IFS: Integrated Forecasting System (IFS) of the European Centre for Medium-Range Weather Forecasts (ECMWF).

	HALO	FAAM	HOP	CAMS	EMAC	MECO	CESM2	Box	IFS
CO_2	x	x	x		x	x			
CH_4	x	x	x	x	x	x	x		
O_3	xx		x	x	x	x	x		
CO	x	x	x	x	x	x	x		
NO	x	x	x	x	x	x	x		
NO_2	x	x	x	x	x	x	x	x	
HONO	x				x	x	x		
HNO_3	x			x	x	x	x		
PAN	(x)			x	x	x	x		
NOy	x				x	x	x		
J_{NO2}, J_{O1D}, …	x		x		x	x	x		
SO_2	x			x	x	x	x		
RO_2	x				x	x	x		
Org aerosol	x	x	x	x			x		
NO_3 aerosol	x	x	x				x		
SO_4 aerosol	x	x	x	x			x		
NH_4 aerosol	x	x	x				x		
Chl aerosol	x	x	x	x			x		
Org44 aerosol	x	x	x				x		
BCm aerosol	x	x	x	x			x		
BCn aerosol	x	x	x				x		
SCn aerosol	x	x	x				x		
CPC	x	x	x						
CH_2O_FOR	xx		x	x	x	x	x		
C_2H_6_ETA		xx	x	x	x	x	x		
CH_3OH_MET	xx		x		x	x	x		
C_2H_4O_ACA	xx		x		x	x	x		
C_3H_6O_ACE	xx		x		x	x	x		
C_5H_8_ISO	xx		x	x	x	x	x		
C_6H_6_BEN	xxx	x	x				x		
C_7H_8_TOL	xxx	x	x				x		
C_8H_{10}_XYL	xxx		x				x		
C_7H_{16}_HEP	x	x	x				x		
CCl_4	x		x		x	x			
H_2O, RH	x	x	x	x	x	x	x		x
U, V, W	x	x	x	x	x	x	x		x
T, p, h, lon, lat	x	x	x	x	x	x	x		x

Overall, about half of the data pairs from the sets of measurements on the two aircraft differ less than their combined error estimates. In most cases, the differences between the measurements are smaller than the deviations between the model results. For some instruments, the comparison led to significant data analysis improvements. The root mean square deviations between the measurements on FAAM and HALO were less than estimated errors for temperature, relative and absolute humidity, CO_2, benzene, vertical and horizontal wind components, and methane. The largest discrepancies were found for some VOCs, sulphate aerosol and black carbon mass and number concentrations. The instrumental accuracy assessment from the comparison results is in Schumann (2020).

S8 Coordinates of the EMeRGe MPC target areas shown in Figure 4

English Channel (purple)
Longitude: [-5.0, 0.5, 0.5, 1.5, 1.5, -5.0, -5.0]
Latitude: [48.0, 48.0, 49.5, 49.5, 50.8, 50.8, 48.0]
North Sea (red)
Longitude: [-0.5, 3.0, 3.0, 4.0, 4.0, -0.5, -0.5]
Latitude: [50.8, 50.8, 51.8, 51.8, 54.8, 54.8, 50.8]
Benelux/Ruhr (orange)
Longitude: [3.0, 49.5]
Latitude: [8.5, 51.8]
Paris (black)
Longitude: [0.5, 47.0]
Latitude: [7.0, 49.5]
Po Valley (cyan)
Longitude: [7.5, 11.0, 11.0, 14.5, 14.5, 7.5, 7.5]
Latitude: [43.5, 43.5, 44.5, 44.5, 46.5, 46.5, 43.5]
Central Italy (blue)
Longitude: [10.0, 16.0, 16.0, 11.0, 11.0, 10.0, 10.0]
Latitude: [40.5, 40.5, 44.5, 44.5, 43.5, 43.5, 40.5]
East Mediterranean (green)
Longitude: [0.5, 38.5]
Latitude: [8.5, 43.5]

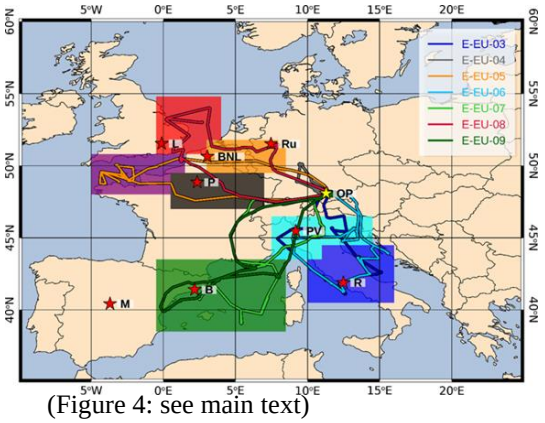

(Figure 4: see main text)

S9 Details of selected flights tracks and flight regions

Table S9.1: Time in UTC and flight levels (FL) of the shuttles and special flight patterns carried out during the EMeRGe flights in the flight region 1. The FL are also given in m for clarity.

Flight region 1	E-EU-03	E-EU-06
Alps	ca. 10:20 UTC FL170, 5100 m ca. 15:50 UTC FL170-240, 5100-7300 m	ca 9:20 UTC FL 170-110, 5100-3300 m 16:20 UTC FL300, 9100 m
MPC Po Valley	10:30 UTC FL110, 3300 m	9:39 UTC and 10:00 UTC FL15/50/100, 450/1500/3000 m 11:50-12:10 UTC; FL25, 750 m
Mediterranean coast of Italy	10:50 UTC FL90, 2700 m	12:20 UTC FL30, 900 m
Shuttle upwind Rome	12:00 UTC FL40/110/150, 1200/3300/4000 m	13:00 UTC FL15/50/100, 450/1500/3000 m
MPC Rome	13:30 UTC; FL 110,3300 m	14:00 UTC FL 100, 3000m
Adriatic coast	13:42 UTC, FL150/110/40, 4600/3300/900 m (to the North FL30, 900 m)	14:15 UTC FL15/50/100, 450/1500/3000 m Croatian coast shuttle 15:15 UTC FL15/50/100, 450/1500/3000 m
Munich		16:50-17:30 UTC Special landing ca 1000 m

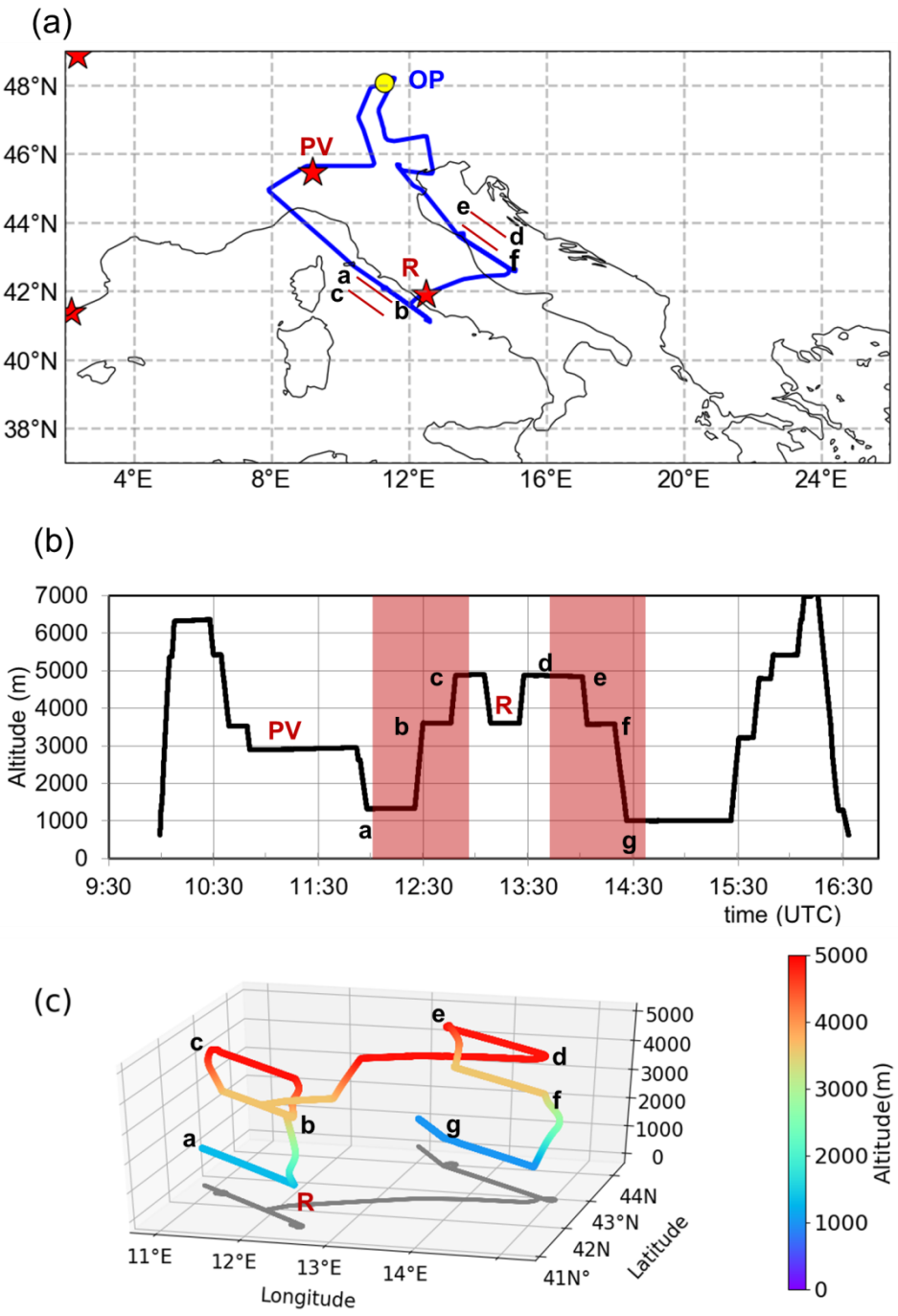

240

241 **Figure S9.1:** Details of the E-EU-03 track on the 11 July 2017. Two shuttles took place upwind Rome (R) and along the
242 Adriatic coast and are marked a) with red lines on the map, b) as red shaded areas on the altitude diagram, and c) as 3-D
243 graph. The flight track during the shuttles is shown in grey. The flight track in a) is coloured as in Fig. 4 and the EMeRGe
244 MPC targets in red. Main changes in course and altitude are marked (a-g) on the graphs for reference. OP indicates the
245 position of the HALO base.

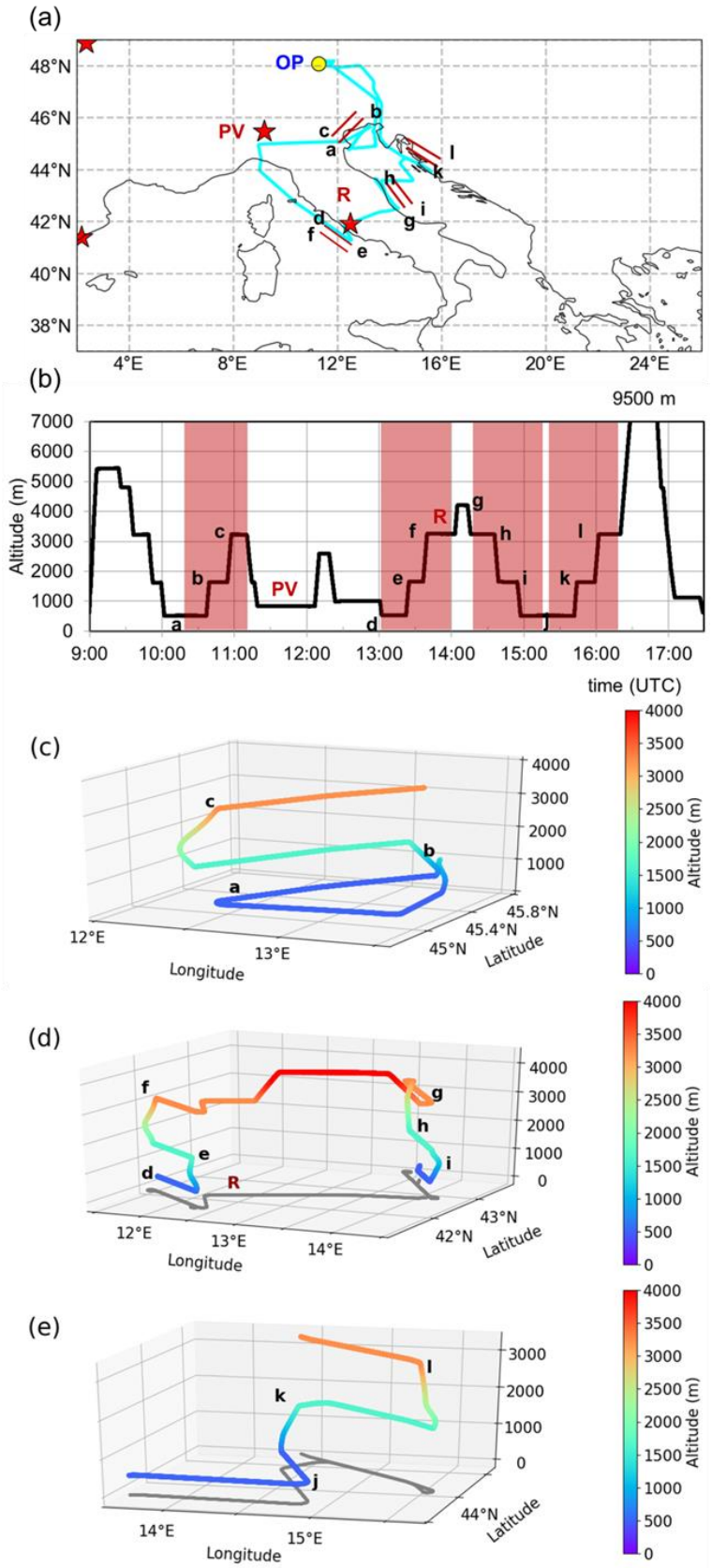

Figure S9.2: Details of the E-EU-06 track on the 20 July 2017. Three shuttles took place downwind of the Po Valley (PV), upwind Rome (R) and along the Adriatic coast and are marked a) with red lines on the map, b) as red shaded areas on the altitude diagram, and c), d) and e) as a 3-D graph. The flight tracks during the shuttles d) and e) are shown in grey. The flight track in a) is coloured as in Fig. 4 and the EMeRGe MPC targets in red. Main changes in course and altitude are marked (a-l) on the graphs for reference. OP indicates the position of the HALO base.

Table S9.2: Time in UTC and flight levels (FL) of the shuttles and special flight patterns carried out during the EMeRGe flights in the flight region 2. The FL are also given in m for clarity.

Flight region 2	**E-EU-05**	**E-EU-08**
MPC BNL/Ruhr	ca. 10:40 UTC FL180, 5500 m	ca. 12:45 -14:30 UTC ~FL80 cloudy Shuttle 13:20 UTC FL 30/50/80, 900/1500/2400 m
MPC London	English Channel 12:00-16:45 UTC FL15-80, 400-2400 m	10:14 UTC (North Sea) FL20/40/200, 600/1200/600 m 13:05 UTC FL30/50/80, 900/1500/2400 m
MPC Paris	17:00 UTC FL70, 2100 m	8:40 UTC FL70, 2100 m
Munich		ca 15:00 UTC Special landing ca 1000 m

Table S9.3: Time in UTC and flight levels (FL) of the special flight patterns carried out during the special case E-EU-04 in the flight region 2. The FL are also given in m for clarity.

Flight region 2 (FAAM_HALO intercomparison exercise E-EU-04)	
Restricted airspace	ca. 10:55 UTC entering race track FL90 (ca 2700 m) FL150/FL90/FL40, 4500/2700/1200 m ca 12:51 UTC end of the exercise
Intercontinental transport pollution/Canada fires	ca. 13:20-14:00 UTC FL230, 7100 m
Munich	ca 14:40 UTC, ca FL30, 1000 m

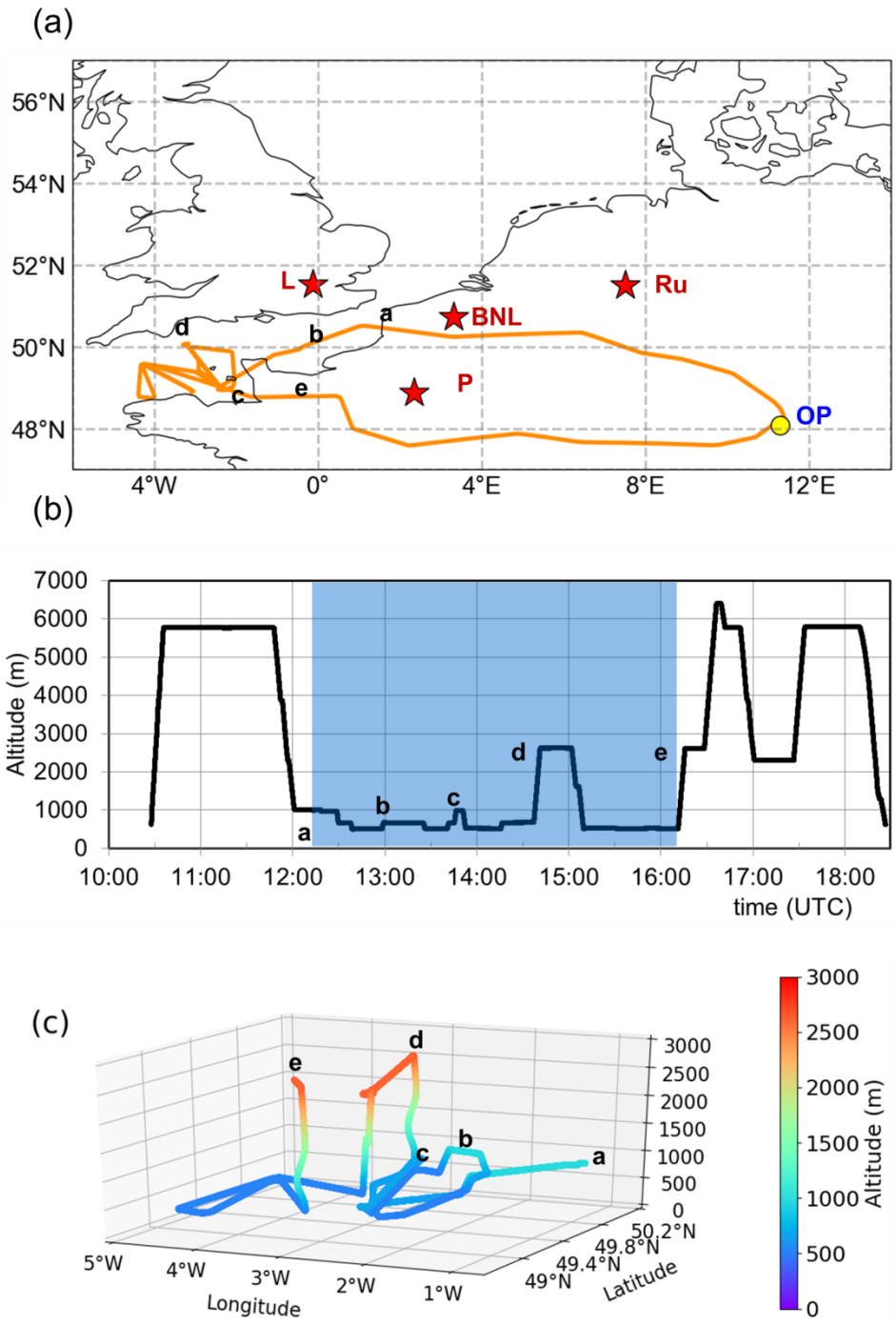

Figure S9.3: Details of the E-EU-05 track on the 17 July 2017. The probing area of the outflow of London over the English Channel is shown in a), as a blue shaded area on the altitude diagram, in b), and as a 3-D graph in c). The flight track in a) is coloured as in Fig. 4 and the EMeRGe MPC targets marked in red. Main changes in course and altitude are marked (a-e) on the graphs for reference. OP indicates the position of the HALO base.

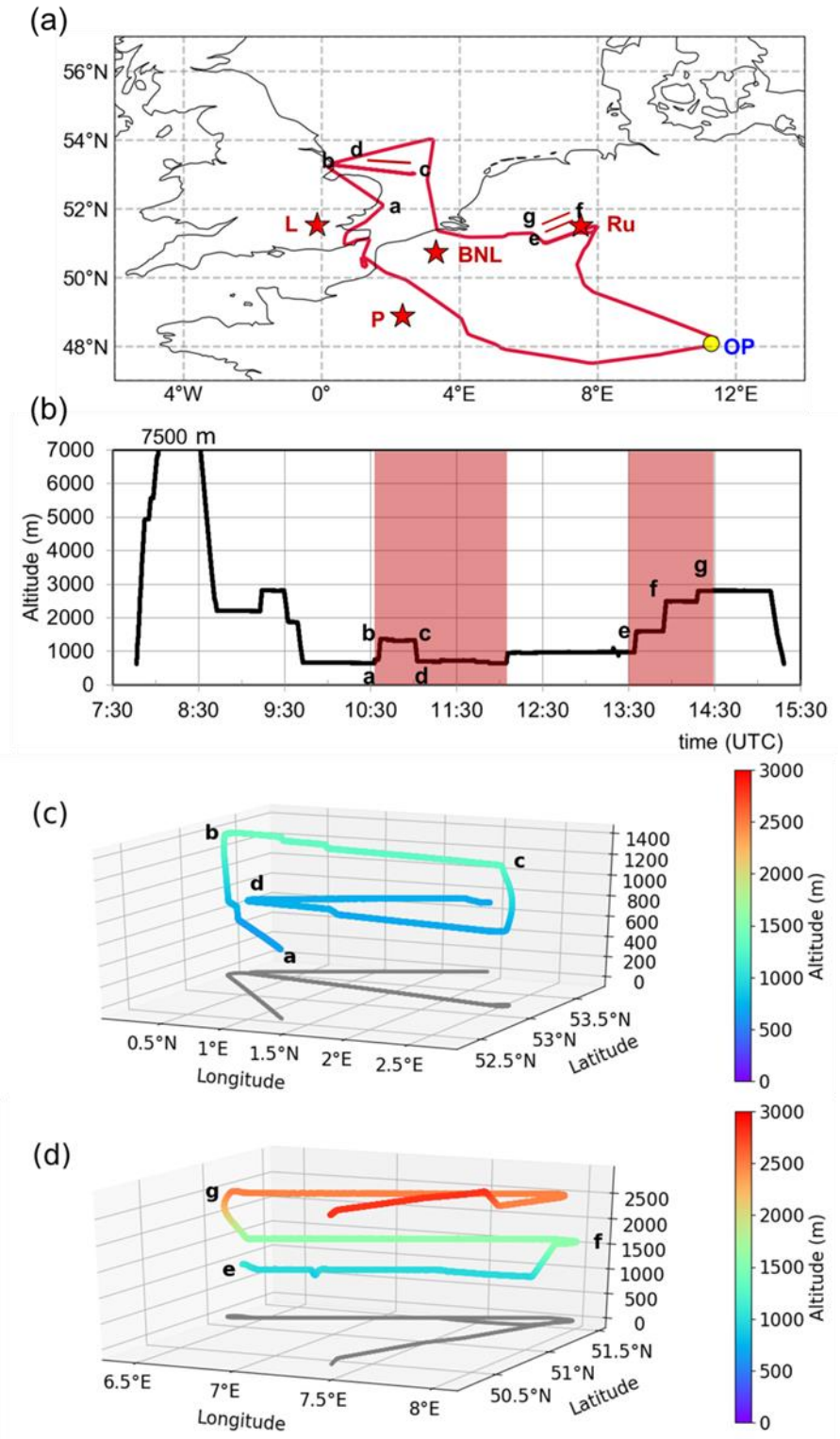

Figure S9.4: Details of the E-EU-08 flight on the 26 July 2017. The position of the shuttles downwind London and the BNL/ Ruhr area are indicated a) in red on the map, b) marked by the red shaded areas, and c), d) as a 3-D graph. The flight tracks during the shuttles are shown in c) and d) in grey. On the map in a) the EMeRGe MPC targets are marked in red and the flight track coloured as in Fig.4. Main changes in course and altitude are marked (a-g) on the graphs for reference. OP indicates the position of the HALO base.

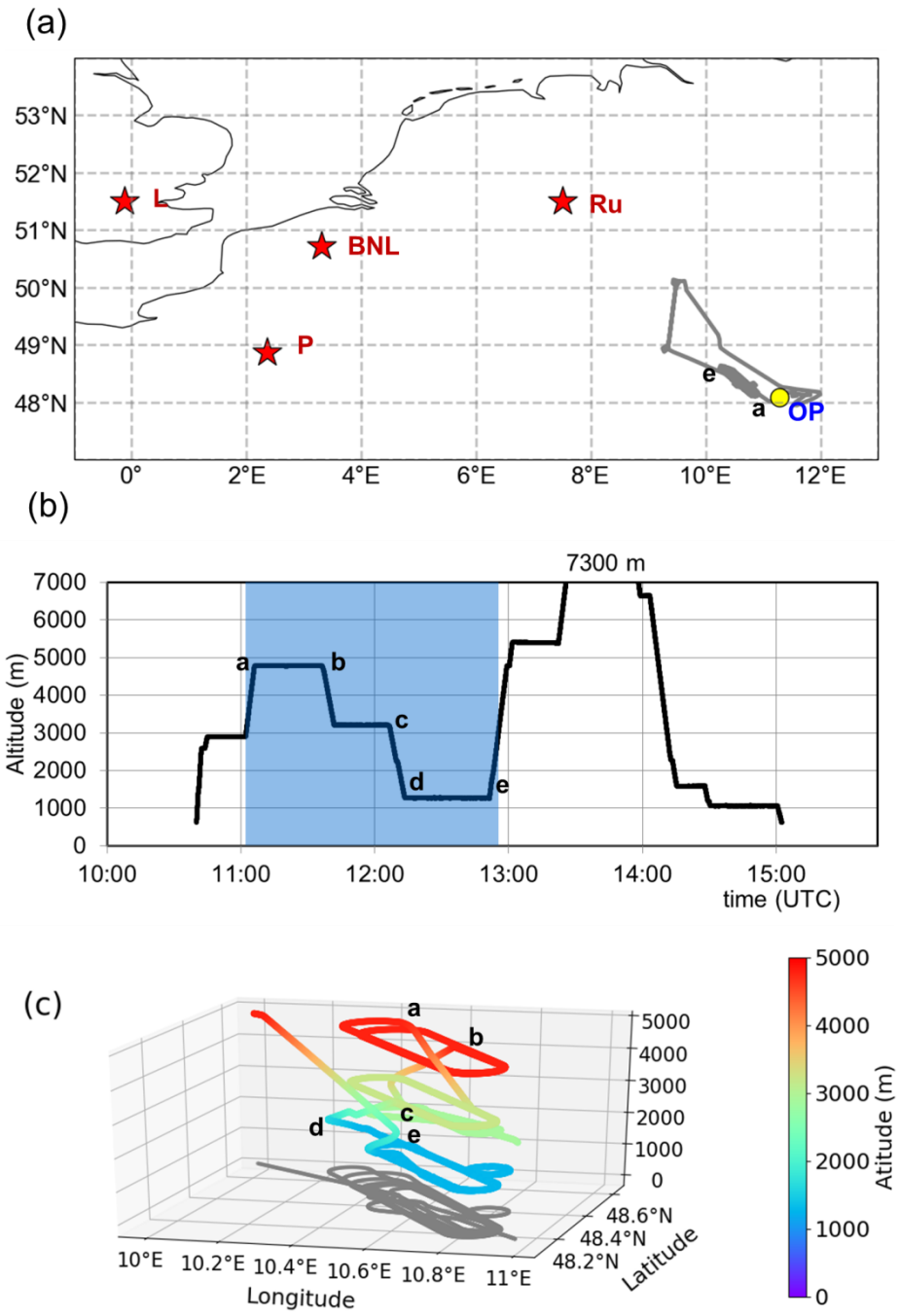

276

277 **Figure S9.5:** Details of the E-EU-04 flight on the 13 July 2017. The flight track coloured as in Fig. 4 is shown on the map in
278 a). The HALO-FAAM intercomparison exercise is indicated by the blue shaded area in b), and as a 3-D graph in c). The
279 flight track is shown in c) in grey. In a), the position of the nearest MPC targets is indicated in red. Main changes in course
280 and altitude are marked (a-d) on the graphs for reference. OP indicates the position of the HALO base.

Table S9.4: Time in UTC and flight levels (FL) of the shuttles and special flight patterns carried out during the EMeRGe flights in the flight region 3. The FL are also given in m for clarity.

Flight region 3	**E-EU-07**	**E-EU-09**
Po Valley	ca. 10:20 UTC FL60, 1800 m	10-11 UTC FL 240,7300 m
Outflow South France (Marseille fires)	11:35 UTC FL90/50/15, 2700/1500/450 m	10:55 UTC FL100/30/15, 300/100/450 m 16:00 UTC FL90, 2700 m
MPC Barcelona	shuttle 12:40 UTC FL50/15, 1500 m/450 m	shuttle 15 UTC coast of Barcelona FL15/50/90, 3000/900/450 m
Mediterranean	ca. 13:30 UTC FL15-50, 450-1500 m 14:50 UTC NW of Sardinia FL15/50/110, 450/1500/3300 m	11:50 UTC FL60, 1800m 13:45 UTC East of Valencia FL100/30/15, 3000/900/450 m
Central France	16:40 UTC FL 200, 6100 m	16:40 UTC FL 200, 6100 m
Munich		18:00-18:30 UTC Special landing ca 1000m

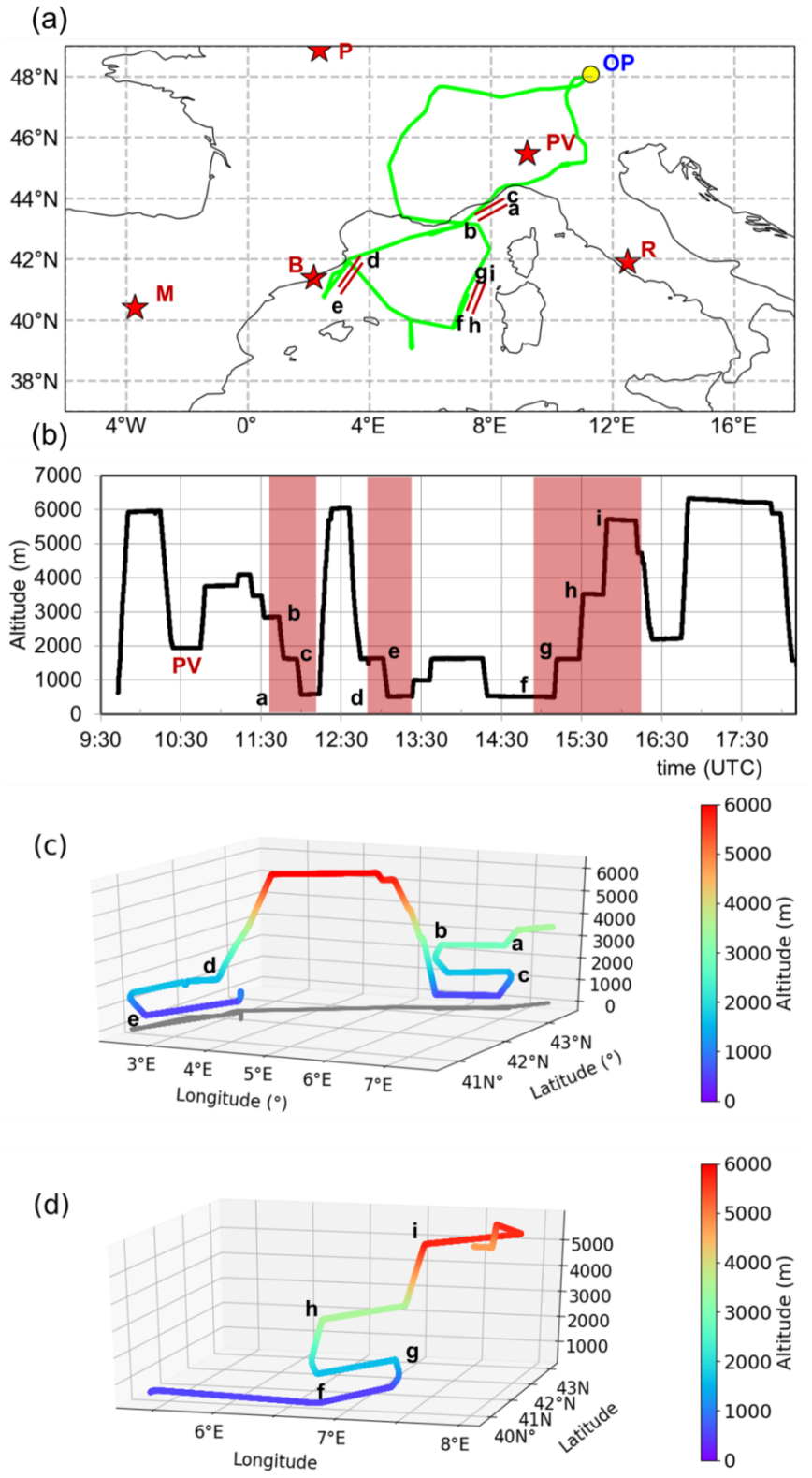

Figure S9.6: Details of the E-EU-07 flight on the 24 July 2017. The position of the shuttles taking place downwind of Marseille, Barcelona and the West coast of Sardinia are indicated in red on the map in a), marked by the red shaded areas in b), and as a 3-D graph depicted in c) and d). The flight tracks during the shuttles are shown in c) and d) in grey. In a) the EMeRGe MPC targets are marked in red and the flight track coloured as in Fig. 4. Main changes in course and altitude are marked (a-i) on the graphs for reference. OP indicates the position of the HALO base.

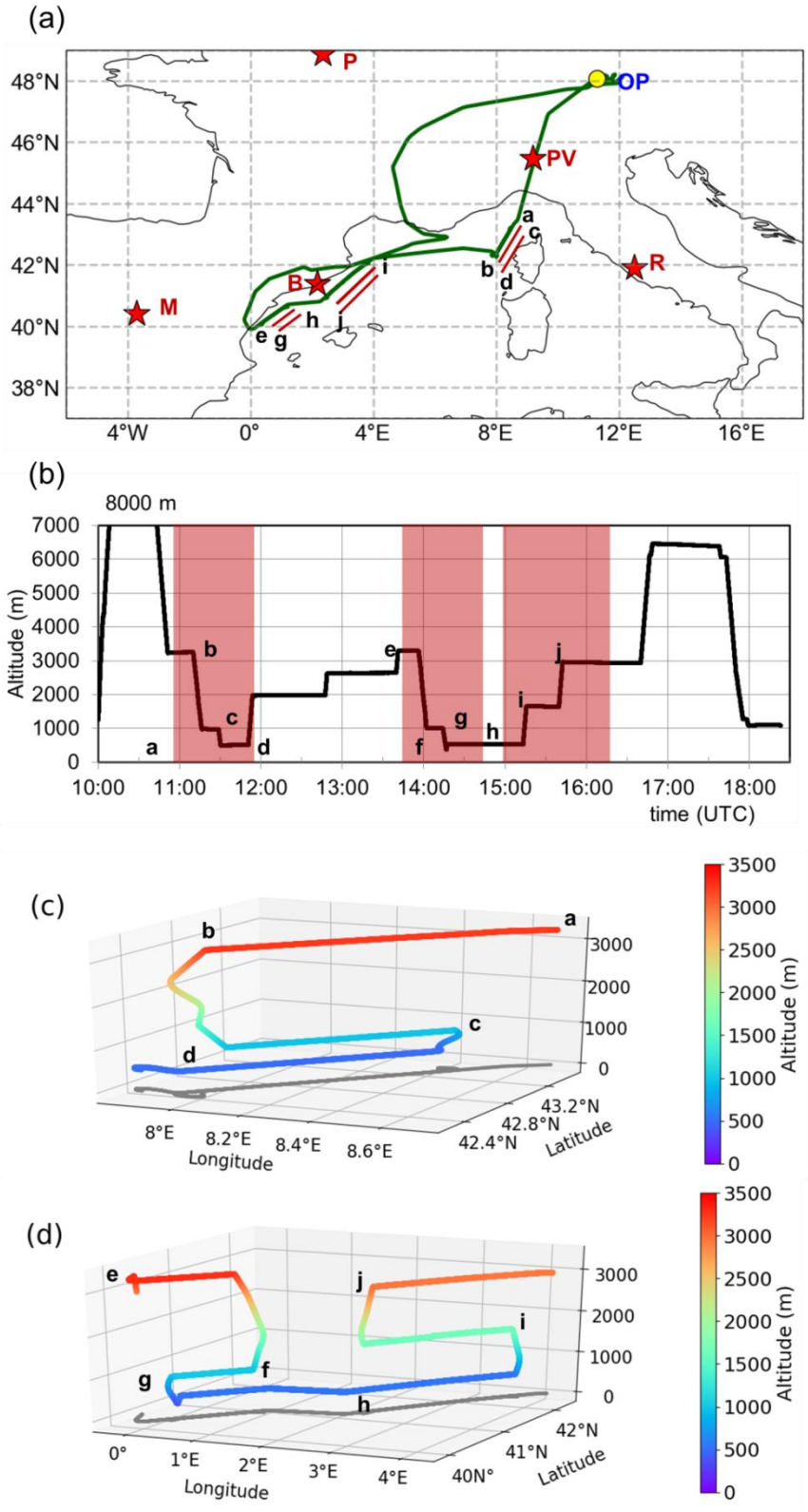

Figure S9.7: Details of the E-EU-09 flight on the 28 July 2017. The position of the shuttles taking place downwind of Marseille, Barcelona and the East coast of Spain are indicated in red on the map in a), marked by the red shaded areas in b), and 3-D depicted in c) and d). The flight tracks during the shuttles are shown in c) and d) in grey. In a) the EMeRGe MPC targets are marked in red and the flight track coloured as in Fig. 4. Main changes in course and altitude are marked (a-j) on the graphs for reference. OP indicates the position of the HALO base.

S10 MODIS fire radiative power

Figure S10.1 shows average fire radiative power observed by MODIS (MODerate resolution Imaging Spectroradiometer, http://modis-fire.umd.edu/) and assimilated within CAMS-global over Europe in July 2017.

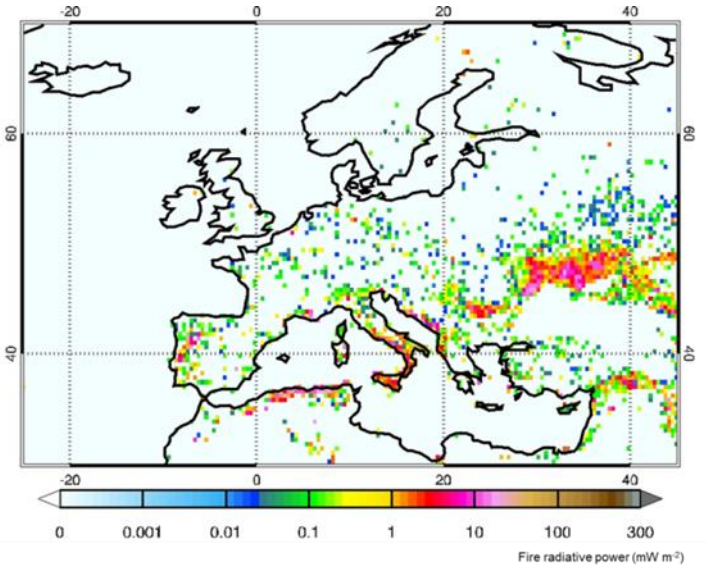

Figure S10.1: Average fire radiative power (mW m^{-2}) as observed by MODIS over Europe in July 2017. Data from the CAMS Global fire assimilation system (GFAS). https://www.ecmwf.int/en/forecasts /dataset/ global-fire-assimilation-system-gfas) fire emission database (see Kaiser et al., 2012).

S11 Selected measured average concentrations for all the EMeRGe flights

Table S11.1: Mean (mean), median (med) and quartiles (25^{th} 75^{th}) concentrations of selected measured trace gases and aerosol particles for the EMeRGe flights: Note that HCHO, NO_2, HONO, CH_2O, $C_2H_2O_2$ and $C_3H_4O_2$ were remotely measured by the mini DOAS instrument; for the averaging volume, see Kluge et al., (2020)[1]. ^{x}HCHO: HCHO from PTRMS measurements; *HCHO: HCHO from miniDOAS measurements; n.a. non-available; N_{CN}: $\mathbf{N_{D>250nm}}$ particle with D> 10 nm, and D>250 nm, respectively (inlet cut-off 1.5 to 3 µm depending on height); BCm: black carbon mass concentration; BCn: black carbon number concentration; OA: Organic aerosol. Note that NCN, N_D, BCm, BCn, OA, NO_3^-, SO_4^{2-}, NH_4^+ and Cl^- are given for standard temperature and pressure conditions.

[1]The averaging volume of the remotely measured NO_2, HONO, CH_2O, $C_2H_2O_2$, and $C_3H_4O_2$ concentrations are given in the vertical by the field of view of the telescope (0.380) (see table 2 in Hüneke et al., 2017) and at clear skies in the horizontal perpendicular to the aircraft flight. They range between 10 km to 25 km near the ground and up to 75 to 100 km at 14 km altitude between 343.7 nm and 477.6 nm, respectively, with considerable shorter (photon path) lengths occurring in the aerosol loaded and cloudy atmosphere (for details see section 2 in Kluge et al., 2020). In flight direction, the skylight spectra are co-added within less than 30 s, which averages over 6 km for a typical aircraft speed of 200 m s^{-1}. Detailed radiative transfer simulations indicated that the averaging kernel in horizontal perpendicular to the aircraft flight direction maximizes for clear skies at about 20 % of the averages, i.e. for 2 to 5 km near ground and 15 km to 20 km at 14 km for 343.7 nm/477.6 nm, respectively (see figure 6.8 in Raecke, 2013), which supported to resolve filaments due to mixing of trace gases in the polar jet (see figure 17 in Oelhaf et al., 2019).

E-EU-03	<2000 m				2000-4000 m				>4000 m				
species	mean	med	25th	75th	mean	med	25th	75th	mean	med	25th	75th	unit
O_3	61.9	63.4	57.4	68.6	60.1	60.1	56.8	63.3	73.7	75.5	63.8	83.9	ppbv
CO	96.7	99.9	86.7	104.5	80.8	85.1	75.9	89	89	88.7	83	95.6	ppbv
NO	144	135	108	167	66	57	39	82	38	36	28	44	pptv
NO_y	1561	1414	880	2035	576	599	340	751	410	409	355	470	pptv
HONO	51	49	35	65	42	25	12	40	5	5	4	6	pptv
NO_2	363	331	120	475	86	60	51	73	44	34	29	49	pptv
*HCHO	1983	2006	1322	2503	751	737	547	914	342	338	288	382	pptv
RO_2^*	58	64	37	78	46	43	34	62	30	26	11	43	pptv
SO_2	n.a.	n.a.	n.a.	n.a.	n.a.	n.a.	n.a.	n.a.	n.a.	n.a.	n.a.	n.a.	pptv
N_{CN}	4478	4309	2232	5951	2142	1835	1084	2777	974	877	771	1031	cm^{-3}
$N_{D>250nm}$	103.3	106.1	55	126.8	48.4	36.6	13.2	82.3	9.8	9	6	11.8	cm^{-3}
BCm	0.215	0.196	0.118	0.279	0.048	0.03	0.01	0.065	0.01	0.005	0.002	0.01	$\mu g\ m^{-3}$
BCn	97	96	54	128	23	16	6	36	4	3	2	5	cm^{-3}
OA	1.992	2.157	1.236	2.543	1.424	1.264	0.549	2.213	0.394	0.394	0.307	0.478	$\mu g\ m^{-3}$
NO_3^-	0.224	0.114	0.07	0.21	0.187	0.184	0.067	0.272	0.044	0.038	0.028	0.05	$\mu g\ m^{-3}$
SO_4^{2-}	1.088	1.115	0.783	1.469	0.386	0.263	0.161	0.551	0.113	0.108	0.092	0.127	$\mu g\ m^{-3}$
NH_4^+	0.521	0.497	0.329	0.659	0.289	0.288	0.139	0.399	0.08	0.072	0.058	0.085	$\mu g\ m^{-3}$
Cl^-	0.03	0.029	0.018	0.039	0.021	0.02	0.017	0.025	0.01	0.01	0.01	0.01	$\mu g\ m^{-3}$
C_3H_6O	2375	2473	1901	2906	1560	1613	1210	1933	1656	1691	1512	1863	pptv
CH_3CN	123	121	104	138	118	120	104	129	140	139	125	156	pptv
C_5H_8	100	93	68	116	66	64	53	75	77	68	57	90	pptv
C_6H_6	115	123	55	162	40	31	24	46	28	27	24	31	pptv
C_7H_8	45	44	23	60	23	21	18	25	28	25	20	31	pptv
^{x}HCHO	2190	2197	1364	2841	816	770	562	1018	469	460	385	551	pptv
$C_2H_2O_2$	183	158	125	219	120	89	58	139	93	90	71	122	pptv
$C_3H_4O_2$	1235	1231	1106	1346	988	806	621	1126	790	758	623	1013	pptv

E-EU-04	<2000 m				2000-4000 m				>4000 m				
species	mean	med	25th	75th	mean	med	25th	75th	mean	med	25th	75th	unit
O_3	45	45	42	48	55	54	51	60	67	69	59	74	ppbv
CO	86	86	84	89	79	79	78	80	94	89	87	99	ppbv
NO	310	274	220	375	50	40	30	50	41	34	27	43	pptv
NO_y	2078	1885	1651	2419	345	234	166	427	294	273	233	327	pptv
HONO	75	73	68	82	19	17	11	24	11	11	8	13	pptv
NO_2	722	544	423	964	72	59	49	78	32	32	28	35	pptv
*HCHO	1251	1196	1147	1431	375	347	314	411	169	168	150	182	pptv
RO_2^*	21	24	8	30	29	29	20	36	19	18	8	28	pptv
SO_2	181	176	154	202	111	107	100	119	107	106	97	115	pptv
N_{CN}	9619	7905	4444	13898	928	691	587	849	1701	1172	980	1632	cm^{-3}
$N_{D>250nm}$	68.8	67.6	54.4	80.7	7.6	6	4.7	8.1	8.9	7.3	5.8	10	cm^{-3}
BCm	0.08	0.06	0.04	0.09	0.01	0.00	0.00	0.01	0.01	0.00	0.00	0.01	$\mu g\ m^{-3}$
BCn	44	39	31	52	3	2	1	4	3	2	1	4	cm^{-3}
OA	1.47	1.45	1.33	1.59	0.37	0.33	0.27	0.40	0.56	0.51	0.41	0.71	$\mu g\ m^{-3}$
NO_3^-	0.73	0.70	0.54	0.82	0.13	0.03	0.03	0.04	0.04	0.04	0.03	0.05	$\mu g\ m^{-3}$
SO_4^{2-}	0.63	0.62	0.55	0.71	0.18	0.18	0.14	0.22	0.10	0.09	0.07	0.12	$\mu g\ m^{-3}$
NH_4^+	0.49	0.48	0.40	0.55	0.15	0.08	0.05	0.15	0.08	0.07	0.07	0.10	$\mu g\ m^{-3}$
Cl^-	0.05	0.04	0.03	0.06	0.04	0.03	0.03	0.05	n.a.	n.a.	n.a.	n.a.	$\mu g\ m^{-3}$
C_3H_6O	1356	1351	1261	1442	1376	1388	1314	1435	1682	1614	1543	1716	pptv
CH_3CN	69	70	61	80	98	100	88	112	134	132	108	149	pptv
C_5H_8	83	77	63	96	70	68	55	84	75	72	61	90	pptv
C_6H_6	41	38	32	48	30	30	26	35	31	28	23	35	pptv
C_7H_8	40	38	29	48	26	22	19	28	22	21	18	27	pptv
^{x}HCHO	1215	1175	1017	1378	518	515	448	594	487	469	385	607	pptv
$C_2H_2O_2$	168	150	112	208	98	65	28	103	68	71	19	112	pptv
$C_3H_4O_2$	1108	1150	844	1303	806	641	409	866	560	453	250	829	pptv

E-EU-05	<2000 m				2000-4000 m				>4000 m				
species	mean	med	25th	75th	mean	med	25th	75th	mean	med	25th	75th	unit
O_3	32	33	30	35	44	43	36	50	61	58	52	71	ppbv
CO	79	80	76	83	65	63	54	73	63	63	57	67	ppbv
NO	173	109	91	150	57	39	24	58	34	33	27	40	pptv
NO_y	2725	2455	2056	3025	1115	931	751	1175	577	547	280	822	pptv
HONO	8	3	0	15	4	3	0	7	0	0	0	0	pptv
NO_2	275	258	186	339	87	49	34	149	27	29	25	30	pptv
*HCHO	1004	1010	926	1107	613	425	370	914	209	204	185	231	pptv
RO_2^*	25	24	16	31	27	26	19	32	28	28	15	40	pptv
SO_2	111	84	61	116	52	49	39	62	44	42	34	52	pptv
N_{CN}	3545	2833	1843	4555	1681	578	402	2855	852	692	592	935	cm^{-3}
$N_{D>250nm}$	89.9	84.4	45.8	127.8	25.3	9.3	5.1	50.3	3.4	2.6	1.8	3.8	cm^{-3}
BCm	0.11	0.09	0.05	0.14	0.04	0.01	0.00	0.07	0.00	0.00	0.00	0.00	$\mu g\ m^{-3}$
BCn	52	50	28	69	22	4	2	47	2	2	1	3	cm^{-3}
OA	1.44	1.49	0.98	1.86	2.20	2.28	0.39	3.79	0.24	0.21	0.16	0.27	$\mu g\ m^{-3}$
NO_3^-	0.73	0.49	0.24	1.11	0.65	0.49	0.39	0.70	0.02	0.02	0.02	0.03	$\mu g\ m^{-3}$
SO_4^{2-}	0.71	0.69	0.42	0.88	0.29	0.19	0.16	0.51	0.19	0.18	0.12	0.25	$\mu g\ m^{-3}$
NH_4^+	0.54	0.49	0.30	0.73	0.32	0.32	0.09	0.42	0.08	0.08	0.06	0.09	$\mu g\ m^{-3}$
Cl^-	0.04	0.04	0.02	0.06	0.03	0.03	0.02	0.04	n.a.	n.a.	n.a.	n.a.	$\mu g\ m^{-3}$
C_3H_6O	n.a.	n.a.	n.a.	n.a.	n.a.	n.a.	n.a.	n.a.	n.a.	n.a.	n.a.	n.a.	pptv
CH_3CN	n.a.	n.a.	n.a.	n.a.	n.a.	n.a.	n.a.	n.a.	n.a.	n.a.	n.a.	n.a.	pptv
C_5H_8	n.a.	n.a.	n.a.	n.a.	n.a.	n.a.	n.a.	n.a.	n.a.	n.a.	n.a.	n.a.	pptv
C_6H_6	n.a.	n.a.	n.a.	n.a.	n.a.	n.a.	n.a.	n.a.	n.a.	n.a.	n.a.	n.a.	pptv
C_7H_8	n.a.	n.a.	n.a.	n.a.	n.a.	n.a.	n.a.	n.a.	n.a.	n.a.	n.a.	n.a.	pptv
^{x}HCHO	n.a.	n.a.	n.a.	n.a.	n.a.	n.a.	n.a.	n.a.	n.a.	n.a.	n.a.	n.a.	pptv
$C_2H_2O_2$	161	144	106	201	82	59	15	96	66	69	19	109	pptv
$C_3H_4O_2$	1128	1175	884	1318	753	626	416	848	613	585	260	822	pptv

327

E-EU-06	<2000 m				2000-4000 m				>4000 m				
species	mean	med	25th	75th	mean	med	25th	75th	mean	med	25th	75th	unit
O_3	69	71	58	77	52	51	50	52	58	56	53	64	ppbv
CO	111	113	94	125	78	77	73	81	77	78	70	82	ppbv
NO	189	123	84	205	71	56	47	66	483	42	23	136	pptv
NO_y	3321	2542	1701	4104	737	581	465	939	2006	366	283	490	pptv
HONO	15	13	0	27	3	0	0	9	0	0	0	0	pptv
NO_2	454	378	238	531	169	174	115	199	191	172	43	303	pptv
*HCHO	1408	1219	996	1731	709	690	627	748	588	597	580	599	pptv
RO_2^*	49	52	36	63	41	44	30	53	31	38	16	44	pptv
SO_2	673	514	289	877	136	131	113	152	120	85	73	100	pptv
N_{CN}	6136	2943	2052	4823	1493	1291	1147	1496	914	803	603	1185	cm^{-3}
$N_{D>250nm}$	174.2	150	85.8	224.3	49	48.5	41.1	54.9	22.2	16.3	7	30.7	cm^{-3}
BCm	0.30	0.28	0.14	0.40	0.09	0.07	0.05	0.10	0.04	0.02	0.01	0.04	$\mu g\ m^{-3}$
BCn	127	127	65	176	34	33	28	39	11	7	4	18	cm^{-3}
OA	3.12	3.25	2.02	3.92	1.07	1.00	0.73	1.32	0.45	0.34	0.28	0.51	$\mu g\ m^{-3}$
NO_3^-	0.69	0.15	0.09	0.62	0.07	0.06	0.05	0.08	0.07	0.05	0.04	0.08	$\mu g\ m^{-3}$
SO_4^{2-}	1.64	1.49	0.98	1.93	0.59	0.61	0.55	0.68	0.27	0.20	0.11	0.44	$\mu g\ m^{-3}$
NH_4^+	0.82	0.67	0.46	1.04	0.28	0.29	0.24	0.32	0.17	0.17	0.09	0.22	$\mu g\ m^{-3}$
Cl^-	0.04	0.04	0.02	0.05	0.02	0.02	0.01	0.02	0.03	0.03	0.03	0.03	$\mu g\ m^{-3}$
C_3H_6O	2444	2434	1935	2937	1645	1656	1514	1799	1476	1452	1316	1605	pptv
CH_3CN	140	131	115	152	129	131	118	138	135	132	123	145	pptv
C_5H_8	98	78	59	112	62	57	50	64	73	67	55	83	pptv
C_6H_6	109	94	56	152	36	34	25	41	32	30	22	37	pptv
C_7H_8	57	42	25	77	35	25	22	51	32	30	26	37	pptv
^{x}HCHO	1843	1651	1088	2374	891	875	748	993	641	616	491	782	pptv
$C_2H_2O_2$	220	192	132	276	182	103	49	260	101	63	8	111	pptv
$C_3H_4O_2$	1496	1275	1075	1577	1351	790	574	1622	817	571	296	756	pptv

328

E-EU-07	<2000 m				2000-4000 m				>4000 m				
species	mean	med	25th	75th	mean	med	25th	75th	mean	med	25th	75th	unit
O_3	47	46	41	54	51	51	44	56	64	62	58	69	ppbv
CO	105	101	92	109	115	102	92	110	103	106	97	110	ppbv
NO	189	136	110	265	120	67	47	121	283	49	37	72	pptv
NO_y	1335	919	743	1823	904	564	390	729	1140	451	393	604	pptv
HONO	25	16	7	34	9	5	0	16	5	0	0	5	pptv
NO_2	202	172	144	236	161	61	27	152	52	53	24	67	pptv
*HCHO	973	832	720	1245	438	382	323	450	280	265	140	380	pptv
RO_2^*	39	40	29	49	35	33	19	48	26	19	5	32	pptv
SO_2	224	177	118	262	78	66	48	91	60	57	44	73	pptv
N_{CN}	6508	3446	2367	6854	2919	1995	1235	2907	4350	3123	1518	5453	cm^{-3}
$N_{D>250nm}$	99.2	65.1	33.4	111.1	94	15.7	7.8	65.1	11.4	6.1	3.9	11.1	cm^{-3}
BCm	0.12	0.07	0.04	0.12	0.10	0.02	0.01	0.04	0.01	0.01	0.00	0.01	$\mu g\ m^{-3}$
BCn	55	37	21	62	46	9	3	20	5	4	2	6	cm^{-3}
OA	2.34	1.68	1.21	3.12	1.30	0.59	0.36	2.03	0.44	0.35	0.26	0.45	$\mu g\ m^{-3}$
NO_3^-	0.31	0.15	0.08	0.49	0.18	0.08	0.03	0.26	0.07	0.04	0.03	0.06	$\mu g\ m^{-3}$
SO_4^{2-}	0.82	0.85	0.38	1.16	0.25	0.13	0.07	0.30	0.10	0.08	0.05	0.13	$\mu g\ m^{-3}$
NH_4^+	0.46	0.43	0.29	0.62	0.31	0.23	0.15	0.51	0.09	0.08	0.06	0.09	$\mu g\ m^{-3}$
Cl^-	0.09	0.05	0.02	0.16	0.04	0.04	0.02	0.05	0.10	0.10	0.10	0.10	$\mu g\ m^{-3}$
C_3H_6O	1734	1678	1400	1974	1580	1399	1244	1644	1535	1605	1364	1691	pptv
CH_3CN	124	117	103	131	191	139	119	154	132	134	117	149	pptv
C_5H_8	92	69	57	114	170	80	58	108	66	62	54	70	pptv
C_6H_6	81	66	43	94	71	39	29	54	31	29	24	35	pptv
C_7H_8	51	44	34	61	69	26	20	38	32	31	18	43	pptv
^{x}HCHO	1391	1211	903	1684	1015	682	468	925	467	446	385	527	pptv
$C_2H_2O_2$	221	201	141	268	192	116	54	259	132	88	22	172	pptv
$C_3H_4O_2$	1603	1380	1140	1999	1430	808	591	1841	1012	616	430	1255	pptv

329

E-EU-08	<2000 m				2000-4000 m				>4000 m				
species	mean	med	25th	75th	mean	med	25th	75th	mean	med	25th	75th	unit
O_3	43	45	37	49	51	53	49	55	64	63	56	73	ppbv
CO	98	96	92	102	90	91	85	93	94	93	92	96	ppbv
NO	407	225	155	450	138	77	60	108	109	102	82	131	pptv
NO_y	3734	3039	2075	4018	1991	1302	720	1777	4619	3765	2652	5761	pptv
HONO	n.a.	n.a.	n.a.	n.a.	n.a.	n.a.	n.a.	n.a.	n.a.	n.a.	n.a.	n.a.	pptv
NO_2	n.a.	n.a.	n.a.	n.a.	n.a.	n.a.	n.a.	n.a.	n.a.	n.a.	n.a.	n.a.	pptv
*HCHO	n.a.	n.a.	n.a.	n.a.	n.a.	n.a.	n.a.	n.a.	n.a.	n.a.	n.a.	n.a.	pptv
RO_2^*	20	21	10	29	31	28	21	37	19	13	0	35	pptv
SO_2	193	99	68	169	55	54	43	64	55	52	38	68	pptv
N_{CN}	4514	3186	2066	4551	1041	790	582	1245	2900	1635	728	3935	cm^{-3}
$N_{D>250nm}$	119.2	111.5	61.1	161.1	18.2	12.3	6.2	21.8	7.7	4.4	2.3	9.2	cm^{-3}
BCm	0.14	0.12	0.07	0.18	0.02	0.01	0.01	0.03	0.01	0.00	0.00	0.01	$\mu g\ m^{-3}$
BCn	71	68	42	92	10	8	4	13	4	3	2	6	cm^{-3}
OA	1.80	1.88	1.21	2.37	0.58	0.51	0.34	0.71	0.49	0.50	0.36	0.63	$\mu g\ m^{-3}$
NO_3^-	1.21	0.96	0.60	1.68	0.10	0.07	0.05	0.11	0.07	0.06	0.05	0.08	$\mu g\ m^{-3}$
SO_4^{2-}	0.85	0.73	0.56	0.97	0.20	0.18	0.13	0.23	0.09	0.09	0.07	0.11	$\mu g\ m^{-3}$
NH_4^+	0.80	0.65	0.46	1.08	0.16	0.13	0.10	0.19	n.a.	n.a.	n.a.	n.a.	$\mu g\ m^{-3}$
Cl^-	0.09	0.08	0.05	0.12	0.03	0.02	0.01	0.03	0.03	0.03	0.02	0.03	$\mu g\ m^{-3}$
C_3H_6O	1517	1543	1347	1705	1384	1404	1312	1495	1602	1614	1534	1707	pptv
CH_3CN	94	95	80	106	130	126	113	140	130	131	116	147	pptv
C_5H_8	80	68	56	89	61	57	50	65	69	65	56	71	pptv
C_6H_6	64	63	47	78	33	29	25	36	30	27	24	38	pptv
C_7H_8	45	35	25	55	29	24	18	33	22	19	17	24	pptv
^{x}HCHO	1234	1165	937	1461	642	637	538	733	411	407	290	496	pptv
$C_2H_2O_2$	n.a.	n.a.	n.a.	n.a.	n.a.	n.a.	n.a.	n.a.	n.a.	n.a.	n.a.	n.a.	pptv
$C_3H_4O_2$	n.a.	n.a.	n.a.	n.a.	n.a.	n.a.	n.a.	n.a.	n.a.	n.a.	n.a.	n.a.	pptv

330

E-EU-09	<2000 m				2000-4000 m				>4000 m				
species	mean	med	25th	75th	mean	med	25th	75th	mean	med	25th	75th	unit
O_3	46	45	41	53	59	60	51	69	54	53	46	62	ppbv
CO	94	94	89	103	104	102	84	129	65	62	60	64	ppbv
NO	148	135	101	190	84	80	67	95	39	35	27	46	pptv
NO_y	1151	1051	851	1287	827	907	357	1169	331	281	189	379	pptv
HONO	n.a.	n.a.	n.a.	n.a.	n.a.	n.a.	n.a.	n.a.	n.a.	n.a.	n.a.	n.a.	pptv
NO_2	n.a.	n.a.	n.a.	n.a.	n.a.	n.a.	n.a.	n.a.	n.a.	n.a.	n.a.	n.a.	pptv
*HCHO	n.a.	n.a.	n.a.	n.a.	n.a.	n.a.	n.a.	n.a.	n.a.	n.a.	n.a.	n.a.	pptv
RO_2^*	46	48	35	62	53	55	39	66	13	10	1	20	pptv
SO_2	301	287	193	384	203	204	98	281	73	68	54	85	pptv
N_{CN}	4080	3921	2960	4813	2634	3025	865	3493	2282	1465	1125	3191	cm^{-3}
$N_{D>250nm}$	66	65.1	42.8	78.8	133.9	129	12.6	251.2	1.2	0.6	0.2	1.5	cm^{-3}
BCm	0.12	0.10	0.07	0.15	0.33	0.32	0.02	0.57	0.00	0.00	0.00	0.00	$\mu g\ m^{-3}$
BCn	57	52	40	69	97	102	7	165	1	0	0	1	cm^{-3}
OA	2.41	1.89	1.06	3.58	5.47	6.11	4.61	7.27	0.25	0.23	0.19	0.31	$\mu g\ m^{-3}$
NO_3^-	0.22	0.17	0.13	0.27	0.34	0.32	0.23	0.44	n.a.	n.a.	n.a.	n.a.	$\mu g\ m^{-3}$
SO_4^{2-}	0.97	0.66	0.46	1.45	0.36	0.34	0.20	0.50	0.16	0.17	0.12	0.21	$\mu g\ m^{-3}$
NH_4^+	0.45	0.41	0.28	0.60	0.36	0.34	0.26	0.45	0.12	0.12	0.10	0.13	$\mu g\ m^{-3}$
Cl^-	0.05	0.05	0.04	0.06	0.05	0.05	0.04	0.06	0.04	0.04	0.03	0.04	$\mu g\ m^{-3}$
C_3H_6O	1774	1610	1419	2022	1811	1851	1319	2302	915	814	774	955	pptv
CH_3CN	126	126	111	140	168	169	147	192	133	131	118	141	pptv
C_5H_8	72	69	55	84	68	63	54	75	64	60	55	67	pptv
C_6H_6	79	72	54	96	80	81	54	104	33	31	25	35	pptv
C_7H_8	35	28	20	38	25	22	19	27	23	18	17	28	pptv
^{x}HCHO	1418	1369	1209	1555	1136	1201	788	1406	433	421	341	493	pptv
$C_2H_2O_2$	n.a.	n.a.	n.a.	n.a.	n.a.	n.a.	n.a.	n.a.	n.a.	n.a.	n.a.	n.a.	pptv
$C_3H_4O_2$	n.a.	n.a.	n.a.	n.a.	n.a.	n.a.	n.a.	n.a.	n.a.	n.a.	n.a.	n.a.	pptv

S12 Plume identification and tagging used during EMeRGe IOP in Europe

For the identification of plumes observed during the EMeRGe IOP in Europe, plume tagging and identification approaches were complementary used:

I) Enhancement in the concentration of selected atmospheric species

Periods in which large pollution plume events were measured on-board HALO were initially categorised into a) anthropogenic pollution (AP), b) biomass burning (BB), c) mixed plumes and d) biogenic, by using the presence of three selected VOCs with different sources. Signal identification resulted from concentration enhancements of CH_3CN, C_6H_6 and C_5H_8 when being measured significantly, i.e., three times the instrumental noise, over their individual atmospheric background values or the LODs, resulting in thresholds of 184, 49 and 85 ppt, respectively (for a detailed description see Förster et al., 2022). For example, CH_3CN is almost exclusively emitted from BB (de Gouw et al., 2003; Warneke et al., 2010) whereas C_6H_6 is emitted by traffic and petroleum-related industrial activities (Paz et al., 2015) as well as BB (Simpson et al., 2011; Andreae, 2019). Hence, C_6H_6 enhancements in the absence of CH_3CN were used to identify relatively "pure" anthropogenic pollution. Similarly, CH_3CN enhanced plumes in the absence of C_6H_6 were identified as pure or aged BB events. Events with only CH_3CN can originate from mixed sources, as C_6H_6 may have decayed while CH_3CN remains, due to the different atmospheric lifetimes of these two tracers (CH_3CN ~ 6 month, C_6H_6 ~ 10 days). When both VOCs were enhanced, the plumes were considered to have air masses from both BB and AP sources or only from recent BB. Additionally, enhanced concentrations of the short-lived biogenic tracer C_5H_8 were used as indicator for recent contact with the PBL having biogenic sources (Förster et al., 2022).

These large categorised pollution events were then further classified into single plumes by using altitude, water content, wind direction and enhancements in the concentrations of pollution tracers such as CO and NO_y measured on-board HALO. Fine structures or signatures in individual plumes were numbered relative to the main plume event they belonged to. All plumes encountered were numbered using the notation E-EU-FN-S-PL similarly to the flight nomenclature mentioned in Sect. 2.3, i.e., E stands for EMeRGe, EU for the campaign in Europe, FN are 2 digits for the flight number, S is the letter assigned to the identified captured pollution event, and PL are two digits reserved for the plume number within each pollution event.

II) Backward trajectories: last contact with PBL

The origin and history of the plumes probed at each point of the flight track were traced by using highly-resolved backward trajectories calculated by the kinematic trajectory model FLEXTRA (see Stohl et al., 1995, 1999). Parameters calculated using FLEXTRA and meteorological fields were used to assign the origin of the observed plumes to the EMeRGe targets in different parts of the flight tracks. Typically, the last contact to the PBL (lcPBL), i.e., the time when the backward trajectory reaches the PBL the first time, was used in combination with sensitivity trajectories, which provide the probability of contact of a particular air mass with the lower meters of the PBL before the measurement. This information was cross-checked with the estimated age of air masses based on HYSPLIT CO dispersion calculations in III). Air mass back trajectories for the EMeRGe flights were calculated with the FLEXTRA 5.0 trajectory model and using the European Centre for Medium-Range Forecasts (ECMWF) operational data set ERA5 meteorological data at 0.25° horizontal resolution. Trajectories are started every 1 minute of flight time and reach back 10 days. The general content of the model output was enhanced by adding manually other parameters after the simulations (troph, tropp, blh, sp, surf, cwc) which provided additional information over the BL conditions along the trajectory.

Two sets of data are available:

1. Original trajectories of the FLEXTRA runs at the ~10 min temporal resolution along the flight tracks.
2. Interpolated trajectories at a strict 5 min temporal resolution, linearly interpolated from the original trajectories. In the interpolated trajectories the timestamps are the same for all releases / trajectories and the temporal resolution is higher.

III) Forward trajectories: dispersion of MPC outflows

In a similar approach to that used in the forecast procedures (see Sect.3.2 and S3.2), the HYSPLIT dispersion model was used to calculate the dispersion of CO emissions using emission rates from the EDGAR HTAP V2 emission inventory. They are expressed as CO enhancement caused by the selected MPC outflow over the CO background. The performance of FLEXPART and HYSPLIT for the EMeRGe data was compared for case studies within EMeRGe.

IV) Detection of released PFC tracers

Sampling of PMCH from a tracer release in the centre of London during E-EU-05, and from a tracer release in the centre of London and at the University of Wuppertal during E-EU-08, enabled the prediction of the dispersion and the mixing of the targeted MPC outflows in these flights to be compared (see S5).

S13 Identification of plumes in E-EU-08

Table S13.1: Synopsis of identified structures (A and B) and plumes with anthropogenic (AP), biomass burning (BB) and biogenic signatures (BIO), MPC assignments and estimated transport times (Ttime) based on HYSPLIT and FLEXTRA for E-EU-08.

Notation	begin [UTC]	end [UTC]	signature	MPC origin	Ttime [h]
E-EU-08-0-01	07:47:34	07:57:40	BB, BIO		
E-EU-08-A-00	08:32:45	09:19:00			
E-EU-08-A-01	08:32:45	08:42:00	BB		
E-EU-08-A-02	08:46:00	08:54:00	BB		
E-EU-08-A-03	09:14:00	09:19:00	AP, BB		
E-EU-08-B-00	09:41:25	13:56:45			
E-EU-08-B-01	09:41:25	10:17:00	AP, BIO	London	0-3
E-EU-08-B-02	10:17:00	10:39:30	AP, BIO	London	0-3
E-EU-08-B-03	10:39:30	11:10:00	AP, BIO	London	6-24
E-EU-08-B-04	11:14:10	11:25:35	AP, BIO	London	3-6
E-EU-08-B-05	11:25:35	11:45:00	AP, BIO	London	3-6
E-EU-08-B-06	11:45:00	11:53:00	AP	London	12-24
E-EU-08-B-07	11:53:00	12:05:50	AP		
E-EU-08-B-08	12:05:50	12:42:45	AP	London	12-24
E-EU-08-B-09	12:42:45	13:02:00	AP, BIO	London/BNL/Ruhr	12-48/0-6
E-EU-08-B-10	13:06:00	13:14:00	AP, BIO	BNL/Ruhr	0-12
E-EU-08-B-11	13:14:00	13:38:15	AP, BIO	BNL/Ruhr	0-3
E-EU-08-B-12	13:38:15	13:56:45	AP, BIO	BNL/Ruhr	0-3

S14 General description of MECO(n)

The MECO(n) model system (see Kerkweg and Jöckel, 2012a,b, Hofmann et al., 2012, Mertens et al.,2016) consists of the global chemistry-climate model EMAC and the regional chemistry-climate model COSMO-CLM/MESSy. The nesting of COSMO in EMAC is performed during runtime. The boundary conditions which are necessary for the regional model instances are provided by the next coarser resolved model instance. New boundary conditions are provided at every time step of the driving model, and specific events of long-range transport (e.g. from biomass burning) are captured well in the regional refinements.

S14.1 Model dynamics

EMAC and COSMO-CLM/MESSy are chemistry-climate models which calculate the atmospheric dynamics by solving the primitive equations. The global model EMAC applies the spectral core of the global circulation model ECHAM5. The Newtonian relaxation (nudging) is performed in spectral space for the prognostic variables divergence, vorticity, temperature, and the logarithm of the surface pressure. This applied for 48, 6, 24, and 24 h, respectively for the EMeRGe simulations (see Jöckel et al., 2016). The nudging data are linearly interpolated during updates every 6 hours. Usually, ERA-Interim, ECMWF operational analysis or ERA-5 data are used for the nudging. The regional refinements are not nudged towards ECMWF or any other data. As in classical downscaling applications the prognostic variables are relaxed towards the global model (or coarser resolved regional refinements) at the lateral and top boundaries. This means that the regional model can develop to a certain degree its own dynamics.

S.14.2 Chemical kinetics

In total, the mechanism is described by 298 reactions of 188 species. The chemical species and reactions are as described by Jöckel et al. (2016). Basic gas-phase chemistry of ozone, methane, and odd nitrogen, alkanes and alkenes up to C4 are included. Alkynes and aromatics are not considered. Halogen chemistry includes bromine and chlorine species. For the chemistry of isoprene and selected non-methane hydrocarbons (NMHCs), version 1

of the Mainz Isoprene Mechanism (MIM1) based on Pöschl et al. (2000) is used. Heterogeneous reactions of dinitrogen pentoxide (N_2O_5), halogen nitrates ($ClNO_3$, $BrNO_3$), and hypohalous acids (HOCl, HOBr) are also included. All Hg reactions are switched off.

NO_y is defined as: $NO_y = BrNO_2 + BrNO_3 + ClNO_2 + ClNO_3 + HNO + HONO + HNO_3 + HNO_4 + IC_3H_7NO_3 + ISON + LC_4H_9NO_3 + N + 2 \cdot N_2O_5 + NO + NO_2 + NO_3 + NO_3^-{}_{cs} + PAN$.

$NO_3^-{}_{cs}$ is a residual aerosol nitrate as reaction product of the heterogeneous reaction of N_2O_5:

$N_2O_5 \rightarrow 2\ NO_3^-{}_{cs} + 2H^+{}_{cs}$

RO_2 is defined as: $RO_2 = HO_2 + CH_3O_2 + ISOOH + CH_3CO_3 + CH_3COCH_2O_2 + C_2H_5O_2$

S14.3 Aqueous phase chemistry, scavenging, wet and dry deposition

As in Jöckel et al. (2016) aqueous-phase chemistry in clouds and wet deposition are simulated with the help of the combined explicit scavenging submodel SCAV, which calculates the uptake/release to/from the gas and aqueous phase and subsequent wet deposition. In contrast to more simplified schemes, dissociation and aqueous-phase redox reactions are also explicitly calculated, e.g. the sulphur (IV) to sulphur (VI) oxidation, such that the effective exchange between gas and liquid phase is taken into account. The scheme also includes nitric acid (HNO_3) uptake on aerosol and cloud particles. Wet deposition is calculated from the in-cloud (and subsequent conversion of in-cloud to in-precipitation) and in-precipitation chemical concentrations for both large-scale and convective clouds. Dry deposition of chemical species is calculated using the big leaf approach as proposed by Wesely (1989).

S14.4 Simulation set-up

The simulations are performed using MECO(n) in a MECO(3) configuration, meaning three refinements of COSMO-CLM/MESSy are embedded in EMAC: a) 50 km horizontal resolution, 131 x 121 horizontal grid boxes, time step length = 240 s (CM50), b) 12 km horizontal resolution, 245 x 221 horizontal grid boxes, time step length = 120 s (CM12) and c) 7 km resolution, 330 x 310 horizontal grid boxes, time step length = 60 s (CM7).

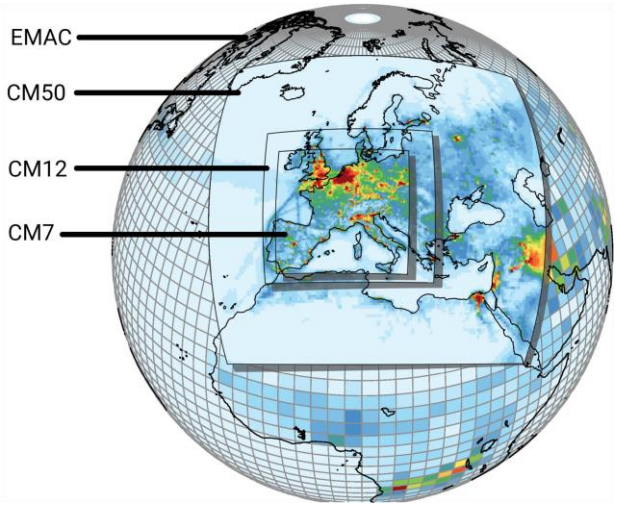

Figure S14.1: Definition of the computational domains of the MECO(3) set-up.

EMAC is applied at a horizontal spectral resolution of T42 (approx. 2.8° x 2.8°) and 90 vertical, terrain following levels from the surface up to approx. 80 km. The time step length is 12 minutes. All COSMO-CLM/MESSy refinements are applied with 40 terrain following vertical levels from the surface up to around 20 km. The results of CM12 and CM7 were not significantly different.

The emission set-up of the reference simulation is the following:

- Long lived greenhouse gases (CO_2, N_2O, CH_4) and CFCs concentrations are relaxed towards prescribed concentrations at surface following the RCP 8.5 emission inventory and zonally averaged.
- Anthropogenic emissions are taken from the 4.3.1 emission inventory (monthly resolution/year 2010).

- Emissions from biomass burning and agricultural waste burning following the RCP 8.5 emission inventory, i.e., it does not correspond the real biomass burning emissions in 2017.
- Emissions of NOx from soils and biogenic VOC are calculated depending on the meteorological conditions following the parametrisations of Yienger and Levy (1995) and Guenther et al. (1995).
- Lightning NOx is parametrised according to Price and Rind (1994).

S14.5 Sensitivity experiments

- emerge3 b (CM50, CM12): Reference simulation with emissions as described above. Nudging of EMAC towards ERA-Interim.
- emerge3 s1 (CM50, CM12, CM7): CH_4 emissions from the EDGAR 4.2 FT emission inventory.
- emerge3 s3 (CM50, CM12): VEU2 emission inventory for anthropogenic emissions are applied for Europe instead of EDGAR 4.3.1
- emerge3 s4 (CM50, CM12): Dynamics in EMAC is nudged towards ECMWF operational analysis data instead of ERA-Interim
- emerge3 s5 (CM50, CM12): 50 instead of 40 vertical model layers increasing vertical resolution in the free troposphere
- emerge3 s6 (CM50, CM12): EDGAR 5.0 emissions for CO_2 and CH_4, diagnostic SO_2 tracer with reaction SO_2 + OH as only loss, additional budget terms for the kinetic calculations.

S14.6 Tagging method for source apportionment

The tagging method used for source apportionment is reported by Grewe et al. (2017) and Rieger et al. (2018). This method is an accounting system which follows the reaction pathways of emissions from different emission sectors. The source apportionment is made for O_3, CO, PAN, NO_y (without PAN), NMHC, OH and HO_2. In this study 12 categories are used (Table S14.1).

Table S14.1. Definition of the tagging categories used for EMeRGe.

Tagging Category	**Description**
Stratosphere	downward transport from the stratosphere
CH_4	degradation of CH_4
Biogenic	biogenic emissions (soil-NOx, biogenic VOCs and CO)
N_2O	degradation of N_2O
Biomass Burning	biomass burning emissions
Lightning	lightning emissions (NOx)
Shipping	shipping emissions (IPCC codes 1A3d + 1C2)
Aviation	aviation emissions
Anth. non-traffic EU	emissions of IPCCs sectors 1A1a, 1A1b + 1B2a5, A1c + 1A5b1 + 1B1b + 1B2a6 + 1B2b5 + 2C1b, 1A2, 1A4, 1B1a + 1B2a1 + 1B2a2 + 1B2a3 + 1B2a4 + 1B2c, 2 + 3, 4B + 4C + 4D + 4F, 6 and 7A in Europa
Anth. non-traffic ROW	emissions of IPCCs sectors 1A1a, 1A1b+1B2a5, 1A1c + 1A5b1 + 1B1b + 1B2a6 + 1B2b5 + 2C1b, 1A2, 1A4, 1B1a + 1B2a1 + 1B2a2 + 1B2a3 + 1B2a4 + 1B2c, 2 + 3, 4B + 4C + 4D + 4F, 6 and 7A in the rest of the world
Landtransport EU	emissions of IPCCs sectors 1A3b + 1A3c + 1A3e in Europe
Landtransport ROW	emissions of IPCCs sectors 1A3b + 1A3c + 1A3e in the rest of the world

S15 References

Andreae, M. O.: Emission of trace gases and aerosols from biomass burning - an updated assessment, Atmos. Chem. Phys., 19, 8523–8546, https://doi.org/10.5194/acp-19-8523-2019, 2019.

Cariolle, D. and Teyssèdre, H.: A revised linear ozone photochemistry parameterization for use in transport and general circulation models: multi-annual simulations, Atmos. Chem. Phys., 7, 2183–2196, https://doi.org/10.5194/acp-7-2183-2007, 2007.

De Gouw, J. A., Warneke, C., Parrish, D. D., Holloway, J. S., Trainer, M., and Fehsenfeld, F. C.: Emission sources and ocean uptake of acetonitrile (CH_3CN) in the atmosphere, J. Geophys. Res., 108, D11, https://doi.org/10.1029/2002JD002897, 2003

Flemming, J., Huijnen, V., Arteta, J., Bechtold, P., Beljaars, A., Blechschmidt, A.-M., Diamantakis, M., Engelen, R. J., Gaudel, A., Inness, A., Jones, L., Josse, B., Katragkou, E., Marecal, V., Peuch, V.-H., Richter, A., Schultz, M. G., Stein, O., and Tsikerdekis, A.: Tropospheric chemistry in the Integrated Forecasting System of ECMWF, Geosci. Model Dev., 8, 975—1003, https://doi.org/10.5194/gmd-8-975-2015, 2015.

Flemming, F., Jones, L., and Blechschmidt, A.-M.: CAMS supports scientific aircraft campaigns, ECMWF Newsletter No.160 – Summer 2019, https://www.ecmwf.int/en/publications/newsletters, 2019

Förster, E., Bönisch, H., Neumaier, M., Obersteiner, F., Zahn, A., Hilboll, A., Kalisz Hedegaard, A. B., Daskalakis, N., Vrekoussis, M., Lichtenstern, M., and Braesicke P.: Chemical and dynamical identification of emission outflows during the HALO campaign EMeRGe in Europe and Asia, in preparation, 2022.

Gioli, B., Miglietta, F., Vaccari, F. P., Zaldei, A., and De Martino, B.: The Sky Arrow ERA, an innovative airborne platform to monitor mass, momentum and energy exchange of ecosystems, Annals of Geophysics., 49, N1, 109-116, https://doi.org/10.4401/ag-3159, 2006.

Grewe, V., Tsati, E., Mertens, M., Frömming, C., and Jöckel, P.: Contribution of emissions to concentrations: the TAGGING 1.0 submodel based on the Modular Earth Submodel System (MESSy 2.52), Geosci. Model Dev., 10, 2615–2633, doi:10.5194/gmd-10-2615-2017,https://www.geosci-model-dev.net/10/2615/2017/, 2017.

Granier, C., Bessagnet, B., Bond, T., D'Angiola, A., Denier van der Gon, H., Frost, G.J., Heil, A., Kaiser, J.W., Kinne, S., Klimont,Z., Kloster, S., Lamarque, J-F., Liousse, C., Masui, T., Meleux, F., Mieville, A., Ohara, T., Raut J-C., Riahi, K., Schultz, M.G., Smith, S.J., Thompson, A., Aardenne, J., Werf, G.R., Vuuren, D.P.: Evolution of anthropogenic and biomass burning emissions of air pollutants at global and regional scales during the 1980–2010 period. Clim Change 109:163–190. doi:10.1007/s10584-011-0154-1, 2011.

Guenther, A., Hewitt, C., E., D., Fall, R. G., C., Graedel, T., Harley, P., Klinger, L., Lerdau, M., McKay, W., Pierce, T., S., B., Steinbrecher, R., Tallamraju, R., Taylor, J., and Zimmermann, P.: A global model of natural volatile organic compound emissions, J. Geophys. Res., 100, 8873–8892, 1995.

Hilboll, A., Richter, A., and Burrows, J. P.: Long-term changes of tropospheric NO_2 over megacities derived from multiple satellite instruments, Atmos. Chem. Phys., 13, 4145—4169, https://doi.org/10.5194/acp-13-4145-2013, 2013.

Hofmann, C., Kerkweg, A., Wernli, H., and Jöckel, P.: The 1-way on-line coupled atmospheric chemistry model system MECO(n) Part 3: Meteorological evaluation of the on-line coupled system, Geosci. Model Dev., 5, 129–147, doi:10.5194/gmd-5-129-2012, http://www.geosci-model-dev.net/5/129/2012/, 2012.

Holben, B. N., Eck, T. F., Slutsker, I., Tanré, D., Buis, J. P., Setzer, A., Vermote, E., Reagan, J. A., Kaufman, Y. J., Nakajima, T., Lavenu, F., Jankowiak, I., and Smirnov, A.: Aeronet – A Federated Instrument Network and Data Archive for Aerosol Characterization, Remote Sens. Environ., 66, 1–16,https://doi.org/10.1016/S0034-4257(98)00031-5, 1998.

Hollingsworth, A. R., Engelen, R. J., Textor, C., Benedetti, A., Boucher, O., Chevallier, F., Dethof, A., Elbern, H., Eskes, H., Flemming, J., Granier, C., Kaiser, J. W., Morcrette, J.-J., Rayner, P., Peuch, V.-H., Rouil, L., Schultz, M. G., Simmons, A. J., and The Gem Consortium: Toward a monitoring and forecasting system for atmospheric composition: The GEMS project, B. Am. Meteorol. Soc., 89, 1147–1164, 2008.

Hüneke, T., Aderhold, O.-A., Bounin, J., Dorf, M., Gentry, E., Grossmann, K., Grooß, J.-U., Hoor, P., Jöckel, P., Kenntner, M., Knapp, M., Knecht, M., Lörks, D., Ludmann, S., Matthes, S., Raecke, R., Reichert, M., Weimar, J., Werner, B., Zahn, A., Ziereis, H., and Pfeilsticker, K.: The novel HALO mini-DOAS instrument: inferring trace gas concentrations from airborne UV/visible limb spectroscopy under all skies using the scaling method, Atmos. Meas. Tech., 10, 4209—4234, https://doi.org/10.5194/amt-10-4209-2017, 2017.

Huijnen, V., Williams, J., van Weele, M., van Noije, T., Krol, M., Dentener, F., Segers, A., Houweling, S., Peters, W., de Laat, J., Boersma, F., Bergamaschi, P., van Velthoven, P., Le Sager, P., Eskes, H., Alkemade, F., Scheele, R., Nédélec, P., and Pätz, H.-W.: The global chemistry transport model TM5: description and evaluation of the tropospheric chemistry version 3.0, Geosci.Model Dev., 3, 445—473, https://doi.org/10.5194/gmd-3-445-2010, 2010.

Inness, A., Blechschmidt, A.-M., Bouarar, I., Chabrillat, S., Crepulja, M., Engelen, R. J., Eskes, H., Flemming, J., Gaudel, A., Hendrick, F., Huijnen, V., Jones, L., Kapsomenakis, J., Katragkou, E., Keppens, A., Langerock, B., de Mazière, M., Melas, D., Parrington, M., Peuch, V. H., Razinger, M., Richter, A., Schultz, M. G., Suttie, M., Thouret, V., Vrekoussis, M., Wagner, A., and Zerefos, C.: Data assimilation of satelliteretrieved ozone, carbon monoxide and nitrogen dioxide with ECMWF's Composition-IFS, Atmos. Chem. Phys., 15, 5275–5303, https://doi.org/10.5194/acp-15-5275-2015, 2015TS64.

Jöckel, P., Tost, H., Pozzer, A., Kunze, M., Kirner, O., Brenninkmeijer, C. A. M., Brinkop, S.,Cai, D. S., Dyroff, C., Eckstein, J., Frank, F., Garny, H., Gottschaldt, K.-D., Graf, P., Grewe,V., Kerkweg, A., Kern, B., Matthes, S., Mertens, M., Meul, S., Neumaier, M., Nützel, M.,Oberländer-Hayn, S., Ruhnke, R., Runde, T., Sander, R., Scharffe, D., and Zahn, A.: EarthSystem Chemistry integrated Modelling (ESCiMo) with the Modular Earth Submodel System(MESSy) version 2.51, Geosci. Model Dev., 9, 1153–1200, doi:10.5194/gmd-9-1153-2016, http://www.geosci-model-dev.net/9/ 1153/2016 /, 2016.

Kaiser, J. W., Heil, A., Andreae, M. O., Benedetti, A., Chubarova, N., Jones, L., Morcrette, J.-J., Razinger, M., Schultz, M. G., Suttie, M., and van der Werf, G. R.: Biomass burning emissions estimated with a global fire assimilation system based on observed fire radiative power, Biogeosciences, 9, 527–554, https://doi.org/10.5194/bg-9-527-2012, 2012.

Kerkweg, A. and Jöckel, P.: The 1-way on-line coupled atmospheric chemistry model system MECO(n) Part 1: Description of the limited-area atmospheric chemistry model COSMO/MESSy, Geosci. Model Dev., 5, 87–110, doi:10.5194/gmd-5-87-2012, http://www.geosci-model-dev.net/5/87/2012/, 2012a.

Kerkweg, A. and Jöckel, P.: The 1-way on-line coupled atmospheric chemistry model system MECO(n) - Part 2: On-line coupling with the Multi-Model-Driver (MMD), Geosci. Model Dev., 5, 111–128, doi:10.5194/gmd-5-111-2012, http://www.geosci-model-dev.net/5/111/2012/, 2012b.

Kluge, F., Hüneke, T., Knecht, M., Lichtenstern, M., Rotermund, M., Schlager, H., Schreiner, B., and Pfeilsticker, K.: Profiling of formaldehyde, glyoxal, methylglyoxal, and CO over the Amazon: normalized excess mixing ratios and related emission factors in biomass burning plumes, Atmos. Chem. Phys., 20, 12363–12389, https://doi.org/10.5194/acp-20-12363-2020, 2020.

Mei, L. L., Rozanov, V., Vountas, M., Burrows, J., Levy, R., and Lotz, W.: Retrieval of aerosol optical properties using MERIS observations: algorithm and some first results, Remote Sens. Environ., 197, 125–140, https://doi.org/10.1016/j.rse.2016.11.015, 2017a.

Mei, L. L., Rozanov, V., Vountas, M., Burrows, J., Levy, R., and Lotz, W.: A Cloud masking algorithm for the XBAER aerosol retrieval using MERIS data, Remote Sens. Environ., Vol 197, pp 141–160, 15 https://doi.org/10.1016/j.rse.2016.11.016, 2017b.

Mertens, M., Kerkweg, A., Jöckel, P., Tost, H., and Hofmann, C.: The 1-way on-line coupled model system MECO(n) – Part 4: 25 Chemical evaluation (based on MESSy v2.52), Geosci. Model Dev., 9, 3545–3567, https://doi.org/10.5194/gmd-9-3545-2016, 2016.

Oelhaf, Hermann, et al., POLSTRACC: Airborne experiment for studying the Polar Stratosphere in a Changing Climate with the high-altitude long-range research aircraft HALO, POLSTRACC: Airborne experiment for studying the Polar Stratosphere in a Changing Climate with the high-altitude long-range research aircraft HALO, Bull. Amer. Meteor. Soc., doi:10.1175/BAMS-D-18-0181.1, 2019.

Pappalardo, G., Amodeo, A., Apituley, A., Comeron, A., Freudenthaler, V., Linné, H., Ansmann, A., Bösenberg, J., D'Amico, G., Mattis, I., Mona, L., Wandinger, U., Amiridis, V., Alados-Arboledas, L., Nicolae, D., and Wiegner, M.: EARLINET: towards an advanced sustainable European aerosol lidar network, Atmos. Meas. Tech., 7, 2389–2409, https://doi.org/10.5194/amt-7-2389-2014, 2014.

Paz, S., Goldstein, P., Kordova-Biezuner, L. et al.TS78: Differences in Benzene Patterns Among Traffic and Industrial Areas and a Prediction Model for Benzene Rates Based on NOx Values, Water Air Soil Poll., 226, 161, https://doi.org/10.1007/s11270-015-2406-6, 2015.

Pöschl, U., von Kuhlmann, R., Poisson, N., and Crutzen, P.: Development and Intercomparison of Condensed Isoprene Oxidation Mechanisms for Global Atmospheric Modeling, J. Atmos. Chem., 37, 29–152,doi:10.1023/A:1006391009798, 2000.

Price, C. and Rind, D.: Modeling Global Lightning Distributions in a General Circulation Model, Mon. Wea. Rev., 122, 1930–1939, doi:10.1175/1520-0493(1994)122h1930:MGLDIAi2.0.CO;2, doi.org/10.1175/1520-0493(1994)122<1930:MGLDIA>2.0.CO;2, 1994.

Raecke, J. R., Atmospheric Spectroscopy of Trace Gases and Water Vapor in the Tropical Tropopause Layerfrom the NASA Global Hawk, Master thesis at the University of Heidelberg, Heidelberg, Germany, 2013 https://www.iup.uni-heidelberg.de/de/researchstratosphere/files/theses/masters/MScThesis_Rasmus_Raecke.pdf

Ren, Y., Schlager, H., and Martin, D.: The Application of TD/GC/NICI–MS with an Al2O3-PLOT-S Column for the Determination of Perfluoroalkylcycloalkanes in the Atmosphere, Chromatographia, 77, 309–316, https://doi.org/10.1007/s10337-013-2584-6, 2013.

Ren, Y., Baumann, R., and Schlager, H.: An airborne perfluorocarbon tracer system and its first application for a Lagrangian experiment, Atmos. Meas. Tech., 8, 69–80, https://doi.org/10.5194/amt-8-69-2015, 2015.

Richter, A., Burrows, J. P., Nüß, H., Granier, C., and Niemeier, U.: Increase in tropospheric nitrogen dioxide over China observed from space, Nature, 437, 129–132, 70 https://doi.org/10.1038/nature04092, 2005.

Richter, A., Begoin, M., Hilboll, A., and Burrows, J. P.: An improved NO_2 retrieval for the GOME-2 satellite instrument, Atmos. Meas. Tech., 4, 1147–1159, https://doi.org/10.5194/amt-4- 1147-2011, 2011.

Rieger, V. S., Mertens, M., & Grewe, V.: An advanced method of contributing emissions to short-lived chemical species (OH and HO2): the TAGGING 1.1 submodel based on the Modular Earth Submodel System (MESSy 2.53), Geoscientific Model Development, 11, 2049–2066, doi: 10.5194/gmd-11-2049-2018, URL https://www.geosci-model-dev.net/11/2049/2018/. 2018.

Schulz, C., Schneider, J., Amorim Holanda, B., Appel, O., Costa, A., de Sá, S. S., Dreiling, V., Fütterer, D., Jurkat-Witschas, T., Klimach, T., Knote, C., Krämer, M., Martin, S. T., Mertes, S., Pöhlker, M. L., Sauer, D., Voigt, C., Walser, A., Weinzierl, B., Ziereis, H., Zöger, M., Andreae, M. O., Artaxo, P., Machado, L. A. T., Pöschl, U., Wendisch, M., and Borrmann, S.: Aircraft-based observations of isoprene-epoxydiol-derived secondary organic aerosol (IEPOX-SOA) in the tropical upper troposphere over the Amazon region, Atmos. Chem. Phys., 18, 14979–15001, https://doi.org/10.5194/acp-18-14979-2018, 2018.

Schumann, U.: Measurement and model data comparisons for the HALO-FAAM formation flight during EMeRGe on 17 July 2017, Zenodo [data set], https://doi.org/10.5281/zenodo.4427965, 2020

Sindelarova, K., Granier, C., Bouarar, I., Guenther, A., Tilmes, S., Stavrakou, T., Müller, J.-F-., Kuhn, U., Stefani, P. and Knorr, W.: Global data set of biogenic VOC emissions calculated by the MEGAN model over the last 30 years. Atmospheric Chemistry and Physics, 14, 9317-9341. doi:10.5194/acp-14-9317-2014, 2014.

Simpson, I. J., Akagi, S. K., Barletta, B., Blake, N. J., Choi, Y., Diskin, G. S., Fried, A., Fuelberg, H. E., Meinardi, S., Rowland, F. S., Vay, S. A., Weinheimer, A. J., Wennberg, P. O., Wiebring, P., Wisthaler, A., Yang, M., Yokelson, R. J., and Blake, D. R.: Boreal forest fire emissions in fresh Canadian smoke plumes: C1-10 volatile organic compounds (VOCs), CO_2, CO, NO_2, NO, HCN and CH_3CN, Atmos. Chem. Phys., 11, 6445–6463, https://doi.org/10.5194/acp-11-6445-2011, 2011.

Stohl, A., Wotawa, G., Seibert, P., and Kromp-Kolb, H.: Interpolation errors in wind fields as a function of spatial and temporal resolution and their impact on different types of kinematic trajectories, J. Appl. Meteor., 34, 2149–2165, 1995TS90,1995.

Stohl, A., Haimberger, L., Scheele, M. P., and Wernli, H.: An intercomparison of results from three trajectory models, Meteorol. Appl., 8, 127–135, 1999.

Warneke, C., Froyd, K. D., Brioude, J., Bahreini, R., Brock, C. A., Cozic, J., de Gouw, J. A., Fahey, D. W., Ferrare, R., Holloway, J. S., Middlebrook, A. M., Miller, L., Montzka, S., Schwarz, J. P., Sodemann, H., Spackman, J. R., and Stohl, A.: An important contribution to springtime Arctic aerosol from biomass burning in Russia, Geophys. Res. Lett., 37, L01801, https://doi.org/10.1029/2009GL041816, 2010.

Wesely, M.: Parameterization of surface resistances to gaseous dry deposition in regional-scale numerical models, Atmospheric Environment (1967), 23, 1293–1304, doi: http://dx.doi.org/10.1016/0004-6981(89) 90153-4, http://www.sciencedirect.com/ science /article/pii/ 0004698189901534, 1989.

Yienger, J. J. and Levy, H.: Empirical model of global soil-biogenic NOx emissions, J. Geophys. Res. Atmos., 100, 11 447–11 464, doi:10.1029/95JD00370, URL http://dx.doi.org/10.1029/95JD00370, 1995.